https://ntrs.nasa.gov/search.jsp?R=19830025412 2020-03-21T02:51:19+00:00Z

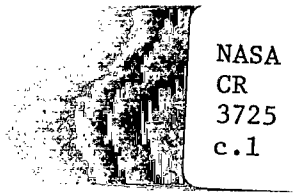

LOAN COPY: RETURN TO
AFWL TECHNICAL LIBRARY
KIRTLAND AFB, N.M. 87117

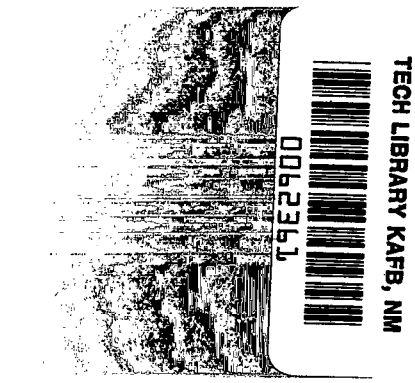

NASA Contractor Report 3725

Experimental Study of the Thermal-Acoustic Efficiency in a Long Turbulent Diffusion-Flame Burner

J. R. Mahan

GRANT NAG3-124
AUGUST 1983

TECH LIBRARY KAFB, NM
0062361

NASA Contractor Report 3725

Experimental Study of the Thermal-Acoustic Efficiency in a Long Turbulent Diffusion-Flame Burner

J. R. Mahan
Virginia Polytechnic Institute and State University
Blacksburg, Virginia

Prepared for
Lewis Research Center
under Grant NAG3-124

NASA
National Aeronautics
and Space Administration

Scientific and Technical
Information Branch

1983

TABLE OF CONTENTS

Experimental Study of the Thermal-Acoustic Efficiency in a Long Turbulent Diffusion-Flame Burner

1. INTRODUCTION

This report describes a two-year study of noise production in a long tubular burner. The research was motivated by an interest in understanding and eventually reducing core noise in gas turbine engines. The general approach is to employ an acoustic source/propagation model to interpret the sound pressure spectrum in the acoustic far field of the burner in terms of the source spectrum that must have produced it. In the model the sources are assumed to be due uniquely to the unsteady component of combustion heat release; thus only direct combustion-noise is considered. The source spectrum is then the variation with frequency of the thermal-acoustic efficiency, defined as the fraction of combustion heat release which is converted into acoustic energy at a given frequency.

The thrust of the research was to study the variation of the source spectrum with the design and operating parameters of the burner. The immediate goal, which was only partially realized in the present effort, was to develop a universal model for the spectral distribution of the thermal-acoustic efficiency which could then be used with the acoustic source/propagation model to predict far-field sound pressure spectra for a given burner design. The ultimate goal of such research would be the definition of a general acoustic source/propagation model applicable to a wide range of gas turbine engines. The present research is envisioned as a demonstration of the feasibility of this idea.

2. REVIEW OF PREVIOUS COMBUSTION NOISE RESEARCH

Although much research has been done on combustion noise, conflicting theories still exist concerning the dominant generating mechanisms. Many theories of combustion noise have been formulated since Lighthill's[1] aeroacoustics theory was published in 1952. Strahle[2,3], for example, developed three different theories on the basis of Lighthill's work. Each of these theories is based on fluid mechanics principles and physical reasoning concerning turbulent flame structures. Strahle argues that the far-field sound pressure is directly proportional to the first Eulerian time derivative of the chemical reaction rate integrated over the reacting volume. Due to the inability to explain the directionality of the source, Strahle concludes that the directionality must be explained by other phenomena such as refraction by temperature gradients. Each of the theories developed by Strahle[2,3] is consistent with the monopole behavior and low frequency nature of combustion noise.

In an extension of Lighthill's theory, Dowling[4] was able to explain directionality effects by accounting for variations in the mean temperatures and the flow velocity. As anticipated by Strahle, the refraction effect, which is included through a Green's function, gives the directionality effects missing in references 2 and 3.

Cumpsty[5] addresses the generation of combustion noise due to entropy disturbances. This type of noise generation is caused by hot (or cold) fluid elements passing through the pressure gradients of the turbine assembly. Cumpsty concludes that the entropy noise, which is a form of indirect combustion noise, dominates the low frequency spectrum.

The views of Strahle[2,3] and Cumpsty[5] as to the dominant generating mechanism in combustion noise are in conflict. The support for the direct combustion noise generating mechanism is based mainly on isolated combustion systems. In a paper by Mathews, Rekos, and Nagel[6], a comparison of the two main combustion noise generating mechanisms in isolated combustors shows that the heat release variations caused by the combustion process is the dominant source of noise radiated from the engine exhaust. However, Cumpsty[5] indicates that the indirect combustion noise prediction method used, which is due to Pickett[7], is inadequate for correctly predicting the effects of the turbine stages. A more recent paper by Muthukrishnan, Strahle, and Neale[8] shows that results based on isolated combustors can be misleading. According to their analysis, combustion noise generation is mainly due to direct combustion noise at low exit Mach numbers, whereas at high exit Mach numbers ($M<0.8$) entropy or indirect noise dominates over direct combustion noise.

Experimental research shows that combustion noise occurs mainly at low frequencies and has very little directionality. Motsinger and Emmerling[9] show that for four turboshaft engines ranging in size from 250 to 22,800 H.P., the peak of the combustion noise spectrum occurs between 400 and 500 Hz. Combustion noise spectra for several turbofan and turbojet engines also have peaks between 400 and 500 Hz. The directivity peaks at about 120 deg from the inlet axis for all of the engines tested. Methods for predicting the combustor sound power level, spectrum, and directivity are also given in reference 9.

Mathews and Rekos[10] determine that the combustion spectra for both can-type and annular geometries were similar. Both experimental and analytical studies are presented. The peak frequency is

found to depend upon the type of burner used. For the burners tested, the range of frequencies corresponding to the peak lies between 280 and 500 Hz. The combustion noise directivity pattern obtained from four turbofan engines shows only minor directivity effects. For all of the engines tested, the directivity peaks at about 120 deg from the inlet axis.

Smith and Kilham[11] provide fundamental data on sound generated by premixed open turbulent flames. Several different parameters are varied to determine their effect on combustion noise. Examination of the combustion-noise spectra indicates that the frequencies corresponding to the peaks may be expressed as a constant nondimensional frequency, or a Strouhal number, defined in terms of the exit diameter, the flow and combustion velocities and the frequency of the peak. At low velocities, the directional effects are very weak. However, as the flow rate increases, the directionality of the combustion noise source increases. In addition, the angle of maximum directivity lies between 40 deg and 80 deg from the burner axis, which corresponds to 140 deg to 100 deg from the inlet axis.

Knott[12] provides data on noise generated by turbulent diffusion flames. An annular burner is used with the fuel entering through the outer annulus and the oxidizer through the center tube. Results are presented for several types of fuels. The directional effects are shown to be weak for most of the fuels used. Knott also shows that the acoustical energy produced by combustible gas jets is considerably greater than that emitted by the unburned gas jets.

Shivashankara, Strahle, and Handley[13] report the results of further investigations of the noise generated by open turbulent flames. Scaling laws for the spectral content, the acoustic power

and the thermal-acoustic efficiency are developed for premixed flames. An empirical relationship for the acoustic power is developed using a regression analysis of the experimental data. Similar results are obtained for the three different fuels used. The directionality is shown to be weak for all of the premixed flames. The spectra of the combustion noise are shown to be predominantly of a low frequency nature. The broadband combustion noise has a single peak and a gradual amplitude roll-off on either side of the peak. The use of a Strouhal number to nondimensionalize combustion noise peak frequencies as suggested by Smith and Kilham[11] is shown to be unacceptable.

Strahle and Shivashankara[14] have extended their combustion noise studies to include gas turbine combustors. The results of experiments conducted to determine the acoustic power and spectra emitted from gas turbine combustors exhausting to the atmosphere indicate that the acoustic power radiated is independent of fuel/air ratio at low fuel/air ratios. However, a transition to a linear dependence on fuel/air ratio occurs above a fuel flow for which the primary stabilization region becomes fuel rich. The spectra are shown to depend mainly on the enclosure acoustics. The smoothed combustion spectrum has a marked peak at 400 Hz and weak secondary peaks at 1200 and its harmonics.

Combustion noise characteristics of a can-type combustor are presented by Shivashankara and Crouch[15]. The effects of several different parameters on the spectral content, the directionality, the radiated sound power, and the thermal-acoustic efficiency are given. A relationship between in-duct and far-field sound levels is established. Empirical relationships for the acoustic power output and the thermal-acoustic efficiency are also developed, and

a generalized combustion noise spectrum is given for several test conditions. The generalized spectrum peaks at 315 Hz while the range of the peak frequency is between 200 and 600 Hz. The generalized directionality peaks at 135 deg from the inlet axis. At low exit velocity, the directivity is very weak but increases as the exit velocity increases. Individual spectra show resonant peaks due to the longitudinal modes of the can-type combustor. The thermal-acoustic efficiency of the can-type combustor is two to four orders of magnitude higher than the thermal-acoustic efficiency of the open turbulent flames in reference 9.

Mathews and Rekos[16] develop an improved prediction system for direct combustion noise in turbopropulsion systems. Expressions for peak frequency and acoustic power output are derived based on burner design and performance parameters. Comparison of analytical models with experimental data show good correlation. Generalized curves of the combustion noise spectrum and directivity show similar results to those obtained in references 9, 10, 14, and 15. In addition, resonance peaks also appear in the individual combustion noise spectra.

Strahle and Muthukrishnan[17] report results of tests of fifteen combustors on four different rigs to determine the correlation between the experimental and theoretical acoustic power. A theoretical basis for the correlation is established using the plane wave theory of direct and indirect combustion noise. A comparison of the theoretical and experimental regression analysis results is given. A single correlation formula is shown to be valid over a wide range of acoustic power. It is emphasized that this is a combustor rig correlation for equivalent power in a reflection-free situation. The thrust of this

study is toward combustor rigs; only the sources directly generated by the combustion process or the combustor rig are investigated. In other words, only the direct combustion noise and the vorticity component of the indirect combustion noise are considered; entropy noise is not present in this investigation.

Shivashankara[18] uses a commercially available auxiliary power unit (APU) gas turbine engine and internal-to-far-field correlations to isolate engine core noise sources. Below 400 Hz, direct combustion noise is found to dominate the APU far-field noise. Additional noise generation between the combustion exit and the turbine exit is observed near 375 and 600 Hz. The additional noise generation is apparently due to entropy noise or flow noise in the turbine inlet torus. Within the secondary duct, mixing of the engine exhaust with the cooling air contributes significantly to the far-field APU noise.

Strahle, Muthukrishnan, and Neale[19] investigate experimental and analytical separation of hydrodynamic, entropy, and combustion noise in gas turbine combustors. Both analytical and experimental results indicate that at low Mach numbers, the exterior radiated sound is mostly due to direct combustion noise while at high Mach numbers, entropy noise dominates the direct combustion noise. Analytical results predict that hydrodynamic noise should dominate combustion noise below 150 Hz. However, experimental investigations show that the hydrodynamic noise is only significant below 50 Hz. Attempts at separating combustion and entropy noise between zero and 100 Hz are fruitless because of the high correlation between them in this frequency range.

Miles[20] uses a dynamic system state-space approach to study a ducted combustion system. Procedures for calculating pressure autospectra and cross-spectra are given. Comparison of the measured spectra with the calculated spectra shows good agreement when allowance is made for dispersion and attentuation effects and the boundary conditions are properly specified. Resonant peaks due to the longitudinal duct modes are observed in the autospectra.

Strahle[21] presents a brief introduction to the physics of combustion noise followed by a short introduction to some of the mathematical and physical descriptions of noise. Comparison of experiment and theory for a premixed, gaseous, small jet flame sets the stage for discussion of more complex flame types. Although the physics of the problem are well understood, a lack of knowledge of turbulence details in a turbulent flame makes it impossible to predict noise output and spectral content.

Legendre[22] investigates noise generating mechanisms of a turbulent gas. He relates noise generation to variations in the circulation and diameter of vortex tubes. Density variation in the flow due to the combustion process is also considered. An estimate for the sound source term in turbulent combustion is presented, as is a corresponding wave equation for propagation of sound into the far-field.

Ho and Doyle[23] develop an empirical expression for the prediction of direct combustion noise by correlating the combustion noise with combustion steady-state parameters for a variety of gas turbine engines. The spectral shape and far-field directivity of the combustion noise correlate well with data provided in references 9, 10, 14, 15, and 16. The empirical formula for the prediction of direct combustion noise is found to correlate within 3-5 dB of the experimental data for all of the gas turbine engines tested.

Muthukrishnan, Strahle, and Neale[24] describe experiments conducted to determine the causes of gas turbine combustor noise. Results indicate that direct combustion noise and entropy noise are the only significant sources of far-field noise. Direct combustion noise predominates at higher frequencies (f<800 Hz) while entropy noise predominates at low frequencies. However, the entropy noise has only minor effects overall.

The terminating or radiation impedance at each end of the combustion system is needed as a boundary condition in order to implement any mathematical model for the standing wave structure.

Levine and Schwinger[25] develop an approximate solution for the radiation of sound from a semi-infinite circular pipe with zero wall thickness. The difference between this approximation and the experimental results for a thin-walled pipe at room temperature is minor.

Ando[26] develops an approximate solution for sound radiation from a semi-infinite circular pipe having a finite wall thickness. For a wall thickness of zero, Ando's results are in good agreement with the results of Levine and Schwinger[25]. Ando's approximation has the advantage of being able to vary the wall thickness of the pipe so that any pipe, regardless of thickness, can be analyzed. Neither the Ando nor the Levine and Schwinger approximation takes into account the temperature dependence of the terminating impedance. Since the present investigation involves implementation of the terminating impedance boundary conditions when the exhaust gas temperature is elevated significantly above the ambient temperature, it is important to understand the effect of this temperature difference on impedance. Several attempts have been made to determine the

effect of temperature difference on the terminating impedance; however, investigators have yet to determine the relationship between the temperature and the terminating impedance.

Fricker and Roberts[27] use the classical impedance tube technique to study the acoustic impedance of the open end of a thick-walled tube with hot flow. They show the radiation impedance as a function of both a wavelength parameter ka and a dimensionless frequency $k_o a$. The wave number k in the wavelength parameter depends on both the frequency and the temperature of the gas flowing from the pipe, while the wave number k_o in the frequency parameter is evaluated at a constant temperature of 0°C. Therefore, the frequency parameter depends only on frequency. No justification is given for evaluating k_o at a temperature of 0°C. The experimental results indicate that the radiation resistance and the reflection coefficient are not significantly dependent upon temperature for a given value of the frequency parameter; however, the resistance depends on temperature for a given value of the wavelength parameter. Agreement between experimental results and the theory of Ando[26] is good when the radiation resistance and reflection coefficient are plotted against the frequency parameter.

Cummings[28] also uses the impedance tube technique to investigate the effects of hot flow on the radiation impedance of an unflanged circular duct. Cummings' experimental results are similar to those of Fricker and Roberts in that they indicate a significant effect of temperature on the radiation resistance for a given wavelength parameter while showing no obvious trend in the radiation reactance. Cummings speculates that the normalized reactance represents a plug of air mainly at a temperature near that of the duct exit which

oscillates with the air in the end of the duct. He speculates further that the radiation resistance increases with temperature because the hot jet at the duct exit is equivalent to a continuation of the duct, with the temperature gradient between the duct exit and the ambient temperature acting as a horn to match the terminating impedance to the characteristic impedance of the surrounding medium.

The results of Fricker and Roberts and Cummings have to be used with discretion due to the absence in both cases of an adequate description of the acoustical environment surrounding the open end of the duct.

Cline[29] uses the impedance tube technique to investigate the effects of hot flow on the radiation impedance of an unflanged circular tube. Experimental results indicate that the use of the classical method to measure the acoustic radiation impedance of a tube with nonisentropic flow is in principle invalid because of the distortion of the standing wave pattern by axial temperature gradients. However, the method is valid from a practical standpoint if the temperature gradients are not too extreme. Cline concludes that a valid method has yet to be demonstrated in this case, although he suggests an iterative technique in which an appropriate wave equation is solved subject to an assumed terminating impedance until good agreement is obtained between the computed and observed standing wave structure.

Zorumski[30] extends an equation derived by Morse[31] for the radiation impedance of a vibrating rigid piston to give the generalized radiation impedances of all modes in circular and annular ducts which have arbitrary wall admittance and which terminate in an infinite baffle. He presents an exact equation for the generalized

impedances of axisymmetric ducts with an infinite baffle. The duct-wall admittance is shown to be a significant parameter in the effect of termination reflections.

Johnston and Ogimoto[32,33] develop an approximation for the terminating impedance of a rigid, finite length, unflanged circular duct with negligible wall thickness. Uniform air flow inside and outside of the duct is accounted for in this approximation. Two main differences in the sound field between the finite and semi-infinite duct are noted. First, the far-field directivity pattern changes from a distorted spherical pattern to a lobed pattern. Secondly, the standing wave pattern inside the duct changes due to the added reflections from both ends of the pipe.

Kinsler and Frey[34] discuss the transfer impedance of both a travelling wave and a standing wave. The transfer impedance of a free travelling plane wave along a duct is equal to the characteristic impedance of the medium divided by the cross-sectional area of the duct. In the standing wave case where both incident and reflected waves are present, the acoustic impedance varies from point to point due to the varying phase relationship between the two waves. Thus, the transfer impedance depends upon the terminating impedance, the length of the pipe and the wave number. However, the terminating impedance depends only upon the physical nature of the termination.

It is apparent that noise generation from a combustion process is not well understood. However, some approximate solutions of combustion noise have been postulated. More experimental data and research is needed in this area in order to understand the source mechanisms of combustion noise.

3. DEFINITION OF THE ACOUSTIC SOURCE/PROPAGATION MODEL

The acoustic source/propagation model is based on a first-order perturbation analysis of the one-dimensional unsteady flow of an inviscid ideal gas. The gas is assumed to be thermally nonconducting, although heat loss to the burner walls is allowed through use of a negative volumetric source term in the corresponding steady flow energy equation. There is no attempt in the model to balance chemical species; combustion is treated as a locally known volumetric heating rate in which the chemical composition of the flow remains that of theoretical air.

Because the equations which describe the acoustic field[†] in the burner are linear, the dependent variables can be related at any frequency of interest by a system of linear algebraic equations;

$$\begin{bmatrix} P_{II} \\ V_{II} \\ T_{II} \end{bmatrix} = \begin{bmatrix} \alpha_{11} & \alpha_{12} & \alpha_{13} & \alpha_{14} \\ \alpha_{21} & \alpha_{22} & \alpha_{23} & \alpha_{24} \\ \alpha_{31} & \alpha_{32} & \alpha_{33} & \alpha_{34} \end{bmatrix} \begin{bmatrix} P_I \\ V_I \\ T_I \\ Q \end{bmatrix} , \qquad (1)$$

where the indices I and II refer to any two sections of the combustor where the complex values of pressure P, velocity V and temperature T are defined.[††]

The quantity Q in equations (1) is a complex number whose value depends on frequency and which represents the ratio of the unsteady

---

[†]We refer to the unsteady component of the flow field in the burner, represented mathematically by the perturbation variables, as an "acoustic" field, even in the source region. We recognize that such a designation may be pedagogically incorrect, but it is consistent with the idea of an "acoustic" model.

[††]This "transfer matrix" approach was suggested by E. A. Krejsa[35] on the basis of a similar analysis by J. H. Miles[20].

heat release at that frequency to the total steady heat release. Thus it is the thermal-acoustic efficiency whose distribution with frequency we refer to as the acoustic source spectrum. In representing the source term by a single complex number at a given frequency we are assuming that the local acoustic sources are proportional to the local steady heat release at each frequency. This hypothesis is based on a series of reasonable assumptions, the validities of which remain to be established:

1. Only the local fluctuations of heat release are dominant in producing the local fluctuations of density which give rise to the acoustic waves propagating into the far field as sound (i.e., we consider only the possibility of direct combustion noise).

2. The only significant fluctuations of heat release are those due to the local turbulent mixing of the unburned fuel and air with the hot products of combustion.

3. The local turbulence level (integrated over the burner cross-section) is uniform in the combustion zone.

Convincing arguments in favor of the first two assumptions are presented by Legendre in reference 22 and will not be reiterated here. Although the third assumption is somewhat more questionable, this does not impose a serious limitation on the results obtained if a realistic form is assumed for the axial distribution of steady combustion heat release. For example, in the present study we assume a distribution of the form

$$\bar{q}(x) = \frac{1}{2} q_o \left[1 - \cos(2\pi x/L) \right] , \qquad (2)$$

where q_o is the maximum value of the local steady heat release and L is the length of the combustion zone. This distribution is similar to that actually found in the experimental burner. Moreover, Mahan and Kasper[36] have established that the low frequency acoustic response of a long burner is not very sensitive to the heat release distribution

as long as the correct total amount of heat is released in the combustion zone. Then for the third assumption to be valid from a practical standpoint it is only necessary for the turbulence level to be uniform in the relatively limited region of the combustion zone surrounding the peak in the distribution given by equation (2) in which most of the heat is released.

The elements α_{ij} of the transfer matrix of equations (1) are determined by solving the equations which describe the unsteady one-dimensional flow of an inviscid ideal gas with a distributed heat source:

the continuity equation,

$$\rho_t + \rho v_x + v\rho_x = 0 \quad , \tag{3}$$

the equation of motion,

$$\rho v_t + \rho v v_x + p_x = 0 \quad , \tag{4}$$

the energy equation,

$$\rho c_p T_t + \rho v c_p T_x = p_t + v p_x + q \quad , \tag{5}$$

the thermodynamic equation of state,

$$p = \rho R T \quad , \tag{6}$$

and the calorimetric equation of state,

$$c_p = c_p(T) \quad , \tag{7}$$

where the variation of specific heat with temperature is computed assuming a mixture of 79 per cent nitrogen and 21 per cent oxygen and using the low pressure formulas given by VanWylen and Sonntag[37]. If one makes the usual assumptions that the solutions p, v, T and ρ consist of a steady component which is a function of axial position only and a very much smaller fluctuating component which is a function of both axial position and time, and that the steady solution itself also satisfies equations (3) through (7), there result

$$\left.\begin{aligned} \bar{v}'/\bar{v} + \bar{p}'/\bar{p} - \bar{T}'/\bar{T} &= 0 \quad , \\ \bar{p}\bar{v}\bar{v}' + R\bar{T}\bar{p}' &= 0 \\ \text{and} \qquad \bar{p}\bar{v}c_p\bar{T}' &= R\bar{T}\bar{v}\bar{p}' + R\bar{T}\bar{q} \quad ; \end{aligned}\right\} \tag{8}$$

and

$$\left.\begin{aligned} (\tilde{p} - \tilde{T})_t + \bar{v}(\tilde{p} + \tilde{v} - \tilde{T})_x &= 0 \quad , \\ \tilde{v}_t + (2\tilde{v} - \tilde{T})\bar{v}' + \bar{v}\tilde{v}_x + (R\bar{T}/\bar{v})\tilde{p}_x &= 0 \\ \text{and} \qquad \tilde{T}_t + \bar{v}\tilde{T}_x &= \left(\frac{\gamma-1}{\gamma}\right)\left[\tilde{p}_t + \bar{v}\tilde{p}_x - (\tilde{p} + \tilde{v} - \tilde{q})\bar{q}/\bar{p}\right] . \end{aligned}\right\} \tag{9}$$

In equations (8) and (9) the quantities with overbars ($\bar{}$) are the steady flow variables and the quantities with tildes ($\tilde{}$) are the acoustic variables nondimensionalized by the corresponding steady flow variables. The subscripts t and x indicate partial differentiation with respect to those variables and the prime (') associated with the steady flow variables indicates differentiation with respect to axial position.

Equations (8) can be integrated directly for a specified axial distribution of steady heat release $\bar{q}(x)$ beginning at any section, the burner inlet for example, where initial values of the pressure, temperature and velocity are known. Once these equations have been solved the variable coefficients in the acoustic equations are known. In order to solve the acoustic equations (9), periodic solutions are assumed of the form

$$\left.\begin{aligned} \tilde{p} &= Pe^{i\omega t} \quad , \\ \tilde{v} &= Ve^{i\omega t} \\ \text{and} \qquad \tilde{T} &= Te^{i\omega t} \quad , \\ \text{with} \qquad \tilde{q} &= Qe^{i\omega t} \quad , \end{aligned}\right\} \tag{10}$$

where the quantities P, V, T and Q are complex functions of axial position only. When these assumed forms are introduced into equations (9) there result the ordinary differential equations

$$\left.\begin{aligned} i\omega(P - V) + \bar{V}(P' + V' - T') &= 0 \quad , \\ i\omega V + (2V - T)\bar{V}' + \bar{V}V' + R\bar{T}P'/\bar{V} &= 0 \\ \text{and} \qquad i\omega T + \bar{V}T' &= \left(\frac{\gamma-1}{\gamma}\right)\left[i\omega P + \bar{V}P' - (P + V - Q)\bar{q}/\bar{p}\right] \quad , \end{aligned}\right\} \tag{11}$$

which can be integrated numerically from any section where initial values are known.†

Unfortunately, a straightforward integration of the acoustic equations (11) is not possible because, unlike the case of the steady flow equations (8) for which $\bar{q}$ is specified and the values of $\bar{p}$, $\bar{v}$ and $\bar{T}$ are known at the burner inlet, there is no section where the complex values of P, V and T are known and, of course, it is the variation with frequency of the thermal-acoustic efficiency Q that is sought in this study. It is for this reason that we have adopted the transfer matrix approach represented by equations (1). We can find the elements α_{ij} of the matrix by integrating equations (11) four times using each time a different but linearly independent set of arbitrary initial conditions P_I, V_I, T_I and the source function Q. If, for example, for the first integration the initial values at the inlet of the burner are assumed to be $P_I = 1$, $V_I = T_I = 0$ and the source function is assumed to be $Q = 0$, the first column of coefficients can be expressed in terms of the solutions obtained by integrating along the burner to the open end of the exhaust pipe; i.e., $\alpha_{11} = P_{II}$, $\alpha_{21} = V_{II}$ and $\alpha_{31} = T_{II}$. Once the elements of the transfer matrix have been thus determined for a given frequency, there remain three algebraic equations in seven unknowns: the values of P, V and T at each end of the burner and the value of Q.

---

†Since P, V, T and Q have real and imaginary parts, equations (11) really represent six equations. However, for purposes of the discussion which follows we treat this as a system of three equations.

Three additional equations can be written in terms of the measured acoustic impedance at either end of the burner,

$$Z_I = P_I/V_I \text{ and } Z_{II} = P_{II}/V_{II} \quad , \tag{12}$$

and the isentropic condition at the burner inlet,

$$T_I = \left(\frac{\gamma-1}{\gamma}\right) P_I \quad . \tag{13}$$

The final equation needed to have a determinant system is the relation between the pressure fluctuation at the open end of the exhaust pipe and the acoustic pressure measured at the same frequency in the far field;

$$P_{II} = A(\omega) P_o \quad , \tag{14}$$

where $A(\omega)$ is the appropriate transfer function. In principle, we are now in a position of being able to compute Q using equations (1), (12), (13) and (14) for any frequency ω for which we have measured P_o.

The foregoing analysis pertains to the simple burner configuration without secondary air flow or holes in the liner. A brief discussion of the procedure which must be followed in the case of holes and secondary flows may be found in subsection 6.4. Discussion of Recommendations.

4. IMPLEMENTATION

The experimental apparatus is shown in Fig. 1. The fuel, hydrogen, enters the combustion chamber through a small sonic orifice in the center of a disk around which air is introduced with a swirl component of velocity. The use of a sonic orifice assures that the acoustic-scale pressure fluctuations in the burner cannot modulate the injection of hydrogen, thus avoiding the possibility of combustion "feed" instability. The air, which flows through a silencer before entering the combustion chamber, is metered by a calibrated rotameter. The wake created by the disk and the swirl component of velocity stabilizes the flame.

The products of combustion are vented into an anechoic chamber through an exhaust pipe having the same inside diameter, 54.6 mm, as the combustion chamber. The burner, including the exhaust pipe, is 1.53 m long and penetrates 0.78 m into the anechoic chamber. The flanges which couple the fuel and air injection manifold and the exhaust pipe to the combustion chamber are water cooled, as is that portion of the exhaust pipe outside the anechoic chamber. The anechoic chamber measures 2.3 m × 2.6 m × 4.0 m and is ventilated by a silenced blower whose capacity limits the power level of the burner to a maximum of around 20 kW. The burner power level is computed from the hydrogen flow rate measured using a calibrated rotameter and assuming complete combustion.

Two Bruel and Kjaer 4133 1/2-in. (1.27 cm) microphones are located in the anechoic chamber at a distance of 1.5 m from the open end of the exhaust pipe, one on the axis of the burner and the other at an angle of 45 deg in the vertical plane above the axis. These microphones are connected to B and K 2603 amplifiers

through B and K 2801 preamplifiers. A Zonic 6080 Fast Fourier Transform analyzer interacts with a Tektronix 4052 graphics terminal to produce autospectra from the sound pressure signals measured by the microphones. The system is calibrated using a B and K 4220 pistonphone.

4.1 Measurement of the Burner Terminating Impedances

The classical impedance tube method was used to measure the acoustic impedance at each end of the burner. The measurements were made in the cold burner without flow and the results extended to the cases with combustion using the relation

$$Z = \rho c z \overline{v} / \overline{p} \quad , \tag{15}$$

where ρc is the characteristic impedance corresponding to the local conditions with combustion and z is the specific impedance measured without combustion. There is no need in this study to correct the impedance for flow effects because the Mach number is always less than 0.02 in the burner.

There can be little doubt of the validity of equation (15) at the burner inlet because the conditions there never differ greatly from those without combustion. However, the conditions at the outlet of the exhaust pipe vary significantly with power level. Indeed, the rather steep axial temperature gradient which exists at the end of the burner must cast doubt on the validity of using this method to determine the impedance there. It is possible, for example, that these gradients can alter the degree to which a circular pipe radiates acoustic energy. Two recent studies, discussed below, seem to indicate that this is not the case, although more research is needed to confirm this conclusion.

Fricker and Roberts[27] and Cummings[28] both used the classical impedance tube technique to measure the radiation impedance of a thick-walled tube from which a hot gas flowed into a relatively cold space. In both experiments the flow velocity was too low to significantly influence the radiation impedance. Both the studies show that although the imaginary component of impedance does not seem to be affected by the difference between the gas temperature in the pipe and that in the room, the real component, when expressed as a function of wavelength in the pipe, increases with the temperature of the gas in the pipe. However, when the real component is expressed as a function of frequency rather than wavelength it is relatively independent of the gas temperature in the pipe. This is exactly the behavior predicted by the classical isothermal theory of Ando[26] for a semi-infinite pipe opening into an anechoic space.

The work of Fricker and Roberts and Cummings then seems to indicate that equation (15) is valid for characterizing the radiation impedance at the open end of the exhaust pipe for a given frequency if it can be assumed that the impedance tube method itself is applicable in the case of axial temperature gradients. That this is the case is certainly open to question because the standing wave structure in the tube, assumed to be uniform in the analysis associated with the classical impedance tube technique, is greatly distorted by the presence of axial temperature gradients. In order to study this question we have developed an impedance measurement technique which is independent of the axial temperature distribution in the exhaust duct. We have utilized this technique in a preliminary study to verify the measurements obtained using the classical method.

The apparatus for this preliminary study is shown in Fig. 2. It consists of a Pyrex tube 1.0 m long and having inside and outside diameters of 74.6 and 79.8 mm, respectively. The lower end of the tube is connected to a small settling chamber and the upper end opens into the laboratory. A speaker located in the settling chamber and driven by an oscillator produces a standing wave in the tube at a specified frequency. Near the lower end there is a small natural gas burner which can be displaced along the axis of the tube. Air enters the tube from the settling chamber and mixes with the natural gas, the mixture is burned, and the products of combustion exit from the open end.

The acoustic pressure in the tube downstream of the burner is measured by a probe borrowed from a B and K 4002 impedance tube apparatus. The probe must be introduced from the upper end of the tube because the burner occupies the axis on the other end. Great care has to be taken to assure that the temperature of the probe is constant during the measurements and that the temperature is the same for each measurement. If not, the sensitivity of the probe will be different from one measurement to the next, thus introducing significant scatter in the data. We were able to avoid this potential source of error by plunging the probe rapidly into the tube and obtaining the pressure measurement before the temperature of the probe could change. After each measurement the probe was retracted and allowed to attain its original temperature before the next measurement.

In addition to the local acoustic pressure on the axis of the tube, the temperature of the gas at the exit of the tube and in the laboratory as well as the air and natural gas flows were measured.

The usual approach in the standing wave, or impedance tube, method consists of measuring the maximum and minimum values of the acoustic pressure amplitude in the tube as well as the axial position of the pressure node nearest the open end. Then the radiation impedance is computed from the standing wave ratio and first node position under the assumption that the standing wave pattern is uniform throughout the tube. In general this is true only if the temperature of the gas in the tube is uniform; if there is a significant axial temperature gradient, the values of the maxima and minima as well as the wavelength of the standing wave will vary along the tube, thus jeopardizing the validity of the method. Fricker and Roberts tried to avoid this problem by extrapolating the standing wave ratio measured at several locations along the tube to the end of the tube, but they evidently did not perform a similar correction for the wavelength. Cummings, on the other hand, tried to avoid axial temperature gradients altogether by selectively heating the walls of the tube.

Our approach consists of finding the radiation impedance, for example by iteration, which minimizes the r.m.s. difference between the measured and calculated standing wave patterns. The calculated pattern is obtained by first integrating equations (8), which describe the mean flow, assuming a uniform heat loss to the walls chosen such that the calculated gas temperature at the tube exit is the same as the measured value. Then the acoustic equations (11) are integrated starting at the open end of the tube with the measured value of the acoustic pressure P,[†] with a value

---

[†]This value was slightly adjusted in several cases to improve the agreement between the measured and calculated waveforms, thus avoiding according too much importance to a single member of a set of data.

of the particle velocity V given by equation (12), and with a value of the acoustic temperature T given by equation (13). Because the integration was always terminated before reaching the flame, the value of Q was taken to be zero.

Figure 3 shows the variation of the real and imaginary parts of the radiation impedance as a function of the wave number based on the temperature of the gas in the tube and reduced by the internal radius of the tube for a range of gas temperatures at the tube exit. These results were obtained by applying the classical analysis, which assumes uniform (undistorted) standing waves, to the data obtained as described above. That is, the standing wave ratio and the axial position of the first node have been used without correction for the distortion of the standing wave by the axial temperature gradient. The impedances thus obtained are in qualitative agreement with those of Fricker and Roberts and of Cummings in that the real part increases with the temperature of the gas in the tube for a given reduced wave number. The significant differences which exist between the experiments of Fricker and Roberts and Cummings and our own apparatus preclude the possibility of a quantitative comparison.†

Figure 4 shows the measured and calculated pressure standing wave waveforms for five cases representing a range of heating conditions. In each case the frequency was 1000 Hz, the air entered the tube at a temperature of 17°C and with a mean velocity of 0.25 m/s, and the temperature in the laboratory was 17°C. The thermal conditions in the tube were varied by changing the position

---

†Indeed, there were significant quantitative differences between Fricker and Roberts' results and those of Cummings.

and heating level of the burner and, in one case, by wrapping the tube with thermal insulation. The symbols in the figure represent the measured values and the curves are the theoretical waveforms. The theoretical waveforms were obtained by integrating the acoustic equations starting with initial conditions based on impedances taken from Fig. 3. The good agreement between the experimental and theoretical results in Fig. 4 demonstrates that good values of impedance can be obtained by analyzing the data in the classical way without considering the distortion of the wave. Thus we can conclude that the classical impedance tube method used by Fricker and Roberts and by Cummings, if the data are obtained carefully, gives good results even in the presence of axial temperature gradients, at least for the limited range of frequencies and thermal conditions of this study. Then it seems that we can indeed accept their results and use with confidence equation (15) for converting the impedance measured without combustion to an impedance corresponding to combustion conditions at a given frequency.

The impedances measured at the two ends of the burner are shown in Figs. 5 and 6. The theoretical impedance of Ando also appears in Fig. 6, which shows the magnitude and phase of the specific impedance at the open end of the exhaust pipe. The agreement between experiment and theory is very good above 700 Hz. The divergence which begins below 700 Hz is probably due to the departure of the chamber from anechoic conditions at low frequencies.

4.2 Determination of the Source Spectra

The strategy for solving equations (1) with equations (12) through (14) is as follows. First, the steady flow equations are

integrated subject to known initial conditions and a specified axial heat transfer distribution. In principle these include the pressure, velocity and temperature at the inlet of the burner, the known combustion heat release distributed according to equation (2), the measured heat loss to the flanges and the cooled portion of the exhaust pipe, and the value of the heat loss to the uncooled portion of the exhaust pipe necessary to obtain the measured gas temperature at the open end. In practice, however, a better agreement can be obtained between the frequencies at which peaks occur in the calculated and measured pressure spectra by slightly adjusting the assumed heat loss to the uncooled portion of the exhaust pipe. In fact, the distribution of the pressure peaks with frequency is fairly sensitive to the distribution of heat loss along the burner for a given total value. An obvious improvement to the technique would be to measure this distribution very carefully and with better spatial resolution.

Next an arbitrary value for Q is assumed whose magnitude is constant at Q_o. The six equations in six unknowns which remain after the value of Q has been specified are then solved for each frequency of interest. For these calculations the flame is divided axially into 20 source elements. Then in order to have incoherent sources, 20 spectra were calculated corresponding to a source at each of the source locations along the length of the flame. These 20 spectra were then added together to form what we call the primitive spectrum. The use of incoherent sources is consistent with the idea that the sources are due to turbulence.

After having thus obtained a primitive pressure autospectrum whose peaks align fairly well with those of the measured pressure

autospectrum, the corresponding source spectrum can be calculated from

$$Q(\omega) = P_{II}(\omega)Q_o/P(\omega) \quad , \tag{16}$$

where $P_{II}(\omega)$ is obtained from the measured sound spectrum using equation (14) and $P(\omega)$ is the calculated primitive sound spectrum corresponding to Q_o. The validity of equation (16) is based on the fact that equations (1) are linear. In the results presented in this report a value of unity has been assumed for the transfer function $A(\omega)$ in equation (14). Although this function was not measured, the transfer function between a location 20 cm inside the exhaust pipe and the microphone location was measured. This function was constant at a value of about 0.75 over the frequency range from 150 Hz to 600 Hz, beyond which a meaningful measure could not be obtained because of the presence of a pressure node near the microphone inside the pipe. A value of unity for $A(\omega)$ seems justified in view of the relative proximity of the field microphone to the open end of the pipe and the limited frequency range.

5. RESULTS

5.1 The Measured Spectra

Typical background and air flow noise spectra without combustion corresponding to the three combustion liners used (see Fig. 7) are shown in Figs. 8, 9 and 10. Liner I has no holes, liner II has a ring of four evenly spaced 12.7 mm diameter holes 76.2 mm from the inlet end of the burner, and liner III has a ring of four evenly spaced 12.7 diameter holes 228.8 mm from the inlet end of the burner.

Figures 11 through 16 compare the spectra at the two microphone locations for three different power levels, 4.5, 10.0 and 22.3 kW, for each of the three liners. In all cases in these figures the total air flow is 620 standard liters per minute (SLPM), and in the cases of liners II and III the primary flow through the swirler is 470 SLPM and the secondary flow through the holes in the liner is 150 SLPM. As expected, the 22.3 kW power level always produces the highest spectrum, followed by the 10 kW power level and finally by the 4.5 kW power level. However, the dependance of the acoustic pressure on thermal power is not linear for any of the combustion liners, indicating that the overall thermal-acoustic efficiency of the combustion process is not constant. The noise spectra for the three different power levels converge at high frequencies (~1500 Hz) to the level without combustion (compare with Figs. 8, 9 and 10) for all three combustion liners, indicating that the effects of combustion are limited to low frequencies. Of course, the peaks in the sound spectra correspond to the longitudinal modes of the burner. These modes are rather diffuse for combustion liner II; in fact, it is easy to imagine that there are double peaks, especially at the lower frequencies. This is probably due to the steep temperature gradients

associated with the introduction of secondary air in the flame zone. This possibility is discussed later in this section in connection with the explanation of double peaks observed in the theoretical spectra. The distance between the peaks increases as the power level increases. This is of course due to the temperature dependence of the speed of sound. Comparisons between the sound spectra at the two microphone locations show only minor differences at all power levels and for all three combustion liners. Thus we will limit our study to the spectra obtained from the "on-axis" microphone.

Figure 17 compares the effects of two different air flow rates, 290 and 620 SLPM, for combustion liner I. The longitudinal modes for this combustion liner are very distinct. The higher air flow rate case shows much higher peaks, suggesting that the increased level of turbulence associated with the higher Reynolds number flow enhances the thermal-acoustic efficiency. The lower air flow rate case corresponds to higher mean flow temperatures along the burner and exhaust pipe, thus producing larger distances between the resonant peaks.

Figure 18 compares the effects of three different air flow combinations for combustion liner II. As pointed out in connection with Figs. 13 and 14, the peaks corresponding to the longitudinal modes are not as distinct with this liner as with combustion liner I. The case for which all of the air enters through the swirler has the highest sound pressure level. This is perhaps because the flow Reynolds number at the base of the flame is largest in this case. Even though another case has the same total air flow, the sound pressure level is lower because part of the air flow is introduced through holes in the

liner wall, thus reducing the mean Reynolds number and presumably the turbulence level at the base of the flame. The "jet" velocity through the holes in the liner is much too low to contribute to the turbulence of the flame. The case with the lowest total air flow rate produces the lowest sound pressure level, due probably to the decrease in turbulence.

Figure 19 compares various air flow combinations for combustion liner III. In the frequency range between 500 and 700 Hz where the highest sound pressure levels are obtained, higher primary air flow rates lead to higher sound pressure levels. This lends weight to the argument that the dominant factor for influencing the thermal-acoustic efficiency is the Reynolds number in the flame region. As in all other cases we note that the spectra approach the "no-flame" levels of Figs. 8, 9 and 10 as we approach 1500 Hz.

A direct comparison between the three combustion liners for a power level of 4.5 kW and a total air flow rate of 620 SLPM is shown in Fig. 20. Combustion liner I has the highest sound pressure level of the three liners, presumably because all of the air enters through the swirler. Combustion liner II and III have the same total air flow rate as liner I but a portion is introduced as secondary air through the holes in the liner. Comparing the sound pressure spectra for these latter two liners shows that each produces higher acoustic pressure levels in certain frequency ranges. The frequency interval between resonant peaks is very nearly the same for each of the combustion chambers, indicating that the steady-state temperatures are not significantly different.

Figure 21 compares the sound pressure spectra produced by combustion liners I, II and III for a power level of 10.0 kW and a total

air flow rate of 620 SLPM. The results shown are very similar to those shown in Fig. 20, and thus the same observations can be made. The overall sound pressure level for all three liners has increased, as has the interval between resonant peaks, due to the increased power level and temperature.

Figure 22 compares the spectra produced by combustion liners I, II and III for a power level of 22.3 kW and a total air flow rate of 290 SLPM. As noted previously in the discussion of the lower power level cases, combustion liner I produces the highest noise level over the whole frequency range due, once again, to the fact that all of the air is introduced through the swirler in the head end of the burner. Above 500 Hz the sound pressure level produced using combustion liner III is higher than that corresponding to combustion liner II. This may be due to a "detuning" of the burner as suggested in connection with the discussion of Figs. 13 and 14. In this scenario one can imagine peaks which are broader but still contain as much or even more acoustic energy as the narrower, sharper peaks associated with combustion liners I and III. This is evidently the case, for example, for the peak around 775 Hz in Fig. 22.

Figure 23 compares the spectra produced by combustion liners I, II and III for a power level of 22.3 kW and a total air flow rate of 620 SLPM. Only minor differences occur between the spectra for combustion liners I and III for these, the highest levels of burner power and total air flow rate. However, the peaks as well as the valleys of the sound pressure spectrum corresponding to combustion liner II are significantly lower. Secondary air introduced into the flame region (or the presence of holes there) clearly has the effect of detuning the burner rather than the anticipated effect of increasing the thermal-acoustic efficiency.

Figure 24 compares the spectra produced by combustion liners I, II and III for a power level of 10.0 kW and with all of the 620 SLPM of air introduced through the swirler. The only parameter varied in this figure is the hole pattern in the combustion liners. The sound pressure spectra of combustion liner I dominates over most of the frequency range. This implies that, as might be expected, the presence of holes in the liner tends to detune the burner in much the same way that an expansion chamber exhaust muffler attenuates sound from an internal combustion engine. The hole pattern of combustion liner II surprisingly has a less attenuating effect than that of combustion liner III. Thus comparison of Figs. 23 and 24 leads us to conclude that air flow through the holes of liner II is an additional factor for detuning the burner.

5.2 Recovery of the Thermal-Acoustic Efficiency Spectra

We now apply the data interpretation technique developed in Section 4 to the three sound pressure spectra shown in Fig. 11. The corresponding primitive spectra, calculated using a value of $\sqrt{2} \times 10^{-5}$ for the magnitude of Q_o, are shown in Fig. 25. These calculations were limited to 150 at the low end of the spectrum because the terminating impedances at either end of the burner could not be measured with confidence below this frequency.

There are four obvious differences between the measured spectra of Fig. 11 and the calculated spectra of Fig. 25.

1. The measured spectra generally decrease with frequency while the calculated spectra generally increase.

2. The measured spectra have simple peaks while the calculated spectra have double peaks above a certain frequency.

3. The calculated spectra have larger peak-to-valley differences (and sharper peaks) than the measured spectra.

4. The general depression in the spectra around 700-900 Hz (depending on the burner power level) is much more pronounced in the calculated spectra than in the measured spectra.

The first difference noted above is a direct consequence of the difference between the actual source spectra in the burner and the assumed constant source spectrum Q_o, whereas the other three differences are artifacts of the acoustic model.

The double peaks in the calculated spectrum occur because there are two acoustic lengths in the model which produce resonances in the frequency range of the calculations: the distance between the two ends of the burner and the distance between the open end of the burner and the steep temperature gradient associated with the combustion heat release. The sharp variation of the characteristic impedance ρc associated with this temperature gradient results in significant reflection of acoustic energy at sufficiently short wavelengths, thus producing secondary resonances. As noted previously, this same effect could be produced by secondary flow into the burner through the holes in the liner for the case of liner II. Presumably a third family of peaks would appear at still higher frequencies above the resonant frequency of the short section of the burner between the closed end and the steep temperature gradient. The fact that no obvious secondary peaks appear in the measured spectra indicates that the one-dimensionality assumed by the acoustic model is not strictly valid in the flame zone. Indeed, the flame does not fill the flame tube in the actual burner, thus leaving an annular region surrounding the flame through which acoustic waves can propagate without being influenced by the steep axial temperature gradient in the flame.

The calculated spectra have larger peak-to-valley differences (and sharper peaks) than the measured spectra because the only acoustic loss mechanism in the model is the radiation resistance at either end of the burner. In the actual burner there are other loss mechanisms associated with viscosity and thermal conductivity which further limit the amplitudes of the resonant peaks. These secondary losses are much less important in determining the values of the spectra at antiresonance, i.e., when the burner is detuned. Thus, the values of the source spectra calculated at antiresonance using equation (16) are much more representative than those calculated at or near resonance.

The general depression, or dip, in the spectra especially evident at antiresonance around 700-900 Hz, depending on the burner power level, is a consequence of the Rayleigh criterion[38], the integral form of which requires that pressure disturbances of wavelength λ be amplified according to the value of

$$\int_0^{\lambda} p(x) \cdot q(x)\, dx \quad ,$$

where $p(x)$ is the local acoustic pressure variation and $q(x)$ is the local unsteady heat transfer. The dot $(\cdot)$ indicates a scalar multiplication of complex quantities; that is, the phase relation between p and q must be considered in evaluating the integral. A pressure disturbance of wavelength λ will be amplified for positive values of the integral and damped for negative values while remaining unaffected for a value of zero. Then the depression in the sound pressure autospectra especially evident in the calculated spectra is due to the first alignment with increasing frequency of a standing wave pressure node with the peak in the heat release distribution, a situation which

minimizes the value of this integral. The fact that this effect is barely noticeable in the measured spectra indicates once again the inadequacy of a one-dimensional model in the flame zone; in reality only that portion of the acoustic wave in the center of the tube is subject to the amplification required by Rayleigh's criterion.

The source spectra calculated using equation (16) and the measured and calculated sound pressure autospectra of Figs. 11 and 25 appear in Fig. 26. The ordinate is in decibels referred to the burner power level; that is dB = 10 $\log_{10}(Q)$ where Q is the thermal-acoustic efficiency given by equation (16). The dashed lines represent the actual source spectra calculated using equation (16) but ignoring the secondary peaks in the theoretical spectra, and the solid lines are smooth curves joining the values of the source spectra corresponding to the antiresonances of the sound pressure spectra. Following the above arguments concerning the differences between the measured and calculated sound spectra, the solid curves are more representative of the actual source spectra than the dashed curves. This is especially true at the higher frequencies where secondary loss mechanisms would be increasingly important. The "humps" which occur in all three spectra between 700 and 900 Hz are a result of the departure from one-dimensionality in the flame zone of the real burner as explained above and thus are not really significant.

It is not surprising to see that the source spectra roll off rather steeply with frequency; this is consistent with the idea that the most important source mechanism is turbulent mixing of the unburned fuel and air with the hot products of combustion. The fact that at 1500 Hz the source spectra are down nearly 20 dB from their values at 150 Hz justifies the decision to limit the study to this

frequency range. All three source spectra decrease an order of magnitude between 150 Hz and the beginning of the influence of the hump around 600 Hz. This means that the most significant source activity is limited to the same frequency range, 0 to 600 Hz, typically observed in jet and open flame noise studies.

It is interesting to note that the three source spectra lie within a 5 dB band and in fact intersect at several frequencies. In general the low burner power case produces the lowest source spectrum, but the high power case does not produce the highest spectrum. That the low burner power spectrum rises above the high burner power spectrum beyond 1100 Hz is probably due to the onset of a second hump in the corresponding theoretical sound pressure spectrum for the low power case which occurs when the second pressure node is aligned with the peak in the heat release distribution. This second hump does not appear in the two higher power cases because the increased burner temperature associated with these cases pushes this hump out to higher frequencies. The combined uncertainty of the experimental and theoretical methods employed in this study is such that it is reasonable to conclude that the thermal-acoustic efficiency Q is relatively insensitive to burner power level. This efficiency has a peak value on the order of 10^{-4} at 150 Hz and decreases about two orders of magnitude for a one order of magnitude increase in frequency.

Another interesting aspect of these source spectra is that in all three cases there is a critical frequency near 500 Hz above which the resonant peaks in the corresponding sound pressure spectra produce sharp depressions in the source spectra (dashed lines) but below which the resonant peaks in the sound spectra translate into

sharp peaks in the source spectra. The sharp depressions have already been explained in terms of the exaggerated resonant peaks in the theoretical sound pressure spectra, but how can the peaks in the source spectra below 500 Hz be explained? A possible explanation is that the mixing process is enhanced at low frequencies by the acoustic agitation of the flame. This is consistent with measurements of flame transfer functions reported in the literature[39] which show that flames respond somewhat like amplified first-order systems, with a relatively flat response up to a critical frequency beyond which the response rolls off steeply with frequency.

6. CONCLUSIONS AND RECOMMENDATIONS

6.1 Conclusions

The following conclusions can be drawn from the results of this study:

1. Enhancement of the sound pressure level in the far-field of the experimental burner by the combustion process is limited to frequencies below 1500 Hz. This is true for the combustion heat release range between 4.5 and 22.3 kW and for several hole patterns and air flow distributions in the burner.

2. The sound pressure level in the "active" part of the spectrum (0-1500 Hz) increases with both burner power level and primary air flow rate.

3. The presence of holes in the liner, with and without air flow through these holes, tends to attenuate the sound pressure level in the far field by comparison to the cases without holes.

4. When there is no secondary flow through the holes in the liner, the attenuation of the sound pressure level in the far field mentioned in 3. above is more pronounced for the liner whose hole pattern is located downstream of the flame zone. However, when there is flow through the holes the opposite is ture.

5. The longitudinal mode frequencies are not modified by the inclusion of holes in the liner, except possibly for the case where the hole pattern coincided with the flame zone. In this case there is some evidence of secondary resonances associated with the acoustic length bounded by the hole location and the open end of the burner.

6. The thermal-acoustic efficiency of the experimental burner is not very sensitive to the burner power level, especially at the higher power levels.

7. The thermal-acoustic efficiency has a peak value of about 10^{-4} at low frequencies (~150 Hz) and decreases at an average rate of 20 dB per decade between 150 and 1500 Hz.

8. There is evidence that the turbulent mixing of the unburned fuel and air with the hot products of combustion is enhanced near resonance by acoustic agitation below a critical frequency around 500 Hz.

6.2 Discussion of Conclusions

Conclusions 1 and 2 above tend to reaffirm the importance of turbulence in the flame zone for the conversion of thermal energy to acoustic energy. That is, enhancement of the far-field sound pressure field by combustion is limited to the range of frequencies normally associated with turbulence and jet noise. The rather steep roll-off of the sound spectrum, as well as the source spectrum, between 150 and 1500 Hz is consistent both with the roll-off of turbulent intensity observed in other studies and the decrease with frequency of the flame mobility reported in reference 39 and alluded to in conclusion 8.

Conclusions 3, 4 and 5 tend to indicate that the presence of holes opening into the annular plenum surrounding the flame tube produces a net attenuation not unlike that associated with an expansion chamber exhaust muffler. The fact that flow into the flame zone through the secondary holes tends to attenuate rather than enhance the far-field sound level indicates that the detuning effect is more important than the increased possibility for turbulence associated with this secondary flow. In fact, the results seem to imply that the highest level of turbulence in the flame zone is obtained when all of the air is introduced through the swirler.

The conclusions pertaining to the thermal-acoustic efficiency, numbers 6, 7 and 8, pertain only to the case of the burner without holes in the flame tube; the efficiencies for the cases with holes have not yet been calculated.

6.3 Recommendations

The following recommendations are made on the basis of this study:

1. The analytical acoustic source/propagation model should be upgraded to include the losses associated with viscosity and thermal conductivity.

2. The model should be modified to in some way account for the two-dimensionality of the flame zone. Of course, an alternative would be to modify the experimental burner in such a way as to insure one-dimensional combustion.

3. Calculation of the source spectra should be extended to the cases of combustion liners with hole patterns and secondary air flows.

4. The value of the transfer function $A(\omega)$ in equation (14) should be carefully measured.

5. In future experiments the gas temperature distribution along the burner should be measured and checked against the distribution calculated using equations (8). The wall heat loss distribution $\bar{q}(x)$ should be tailored to insure good agreement between the measured and calculated axial gas temperature distributions.

6. The techniques and ideas developed in this study should be extended to a gas turbine engine.

6.4 Discussion of Recommendations

The first three recommendations can be implemented without further experimental work. Indeed, we are presently in the process of implementing recommendation 3 at ONERA.† We also have plans to implement the first two recommendations, but this will probably not be done until 1983-84.

Extension of the analysis to the cases of the combustion liners with hole patterns and secondary flows, recommendation 3, requires

---

†ONERA = Office National d'Etudes et de Recherches Aérospatiales, the French National Office of Aerospace Research where the Principal Investigator is spending the 1982-83 academic year on sabbatical leave.

only that equations (1) be written and solved for each subsection of the burner bounded by the ends of the burner and the hole locations, including the annular region surrounding the combustion liner. The general approach would otherwise be the same as for the cases without holes. The impedance of the holes themselves will be computed from classical theory as given for example in reference 40.

Recommendation 4 can be implemented easily upon the return of the Principal Investigator to VPI in the Fall of 1983. However, it is expected that this transfer function will be very near to the assumed value of unity over the frequency range of this study.

Recommendation 5 would require further experimental work with the same or a similar apparatus. This would only lead to a refinement of the present results without greatly changing the values already obtained for the source spectra. Thus, this recommendation would only be implemented if a decision was made to continue the experimental program for other good reasons.

Recommendation 6 should only be implemented after recommendations 1, 2 and 3. In this case recommendation 4 concerning measurement of the transfer function $A(\omega)$ would also be implemented. It is strongly urged that recommendation 6 be implemented, either at NASA Lewis or in the gas turbine research laboratory at VPI.

7. REFERENCES

1. Lighthill, M. J., "On Sound Generated Aerodynamically, I. General Theory," Proceedings of the Royal Society, A211, pp. 564-587.

2. Strahle, Warren C., "On Combustion Generated Noise," Journal of Fluid Mechanics, Vol. 49, Part 2, 1971, pp. 399-414.

3. Strahle, Warren C., "Some Results in Combustion Generated Noise," Journal of Sound and Vibration, Vol. 23, No. 1, 1972, pp. 113-125.

4. Dowling, A. P., "Mean Temperature and Flow Effects on Combustion Noise," AIAA Paper 79-059, 1979.

5. Cumpsty, N. A., "Jet Engine Combustion Noise: Pressure, Entropy and Vorticity Perturbations Produced by Unsteady Combustion or Heat Addition," Journal of Sound and Vibration, Vol. 66, No. 4, 1979, pp. 527-544.

6. Mathews, D. C., M. F. Rekos, and R. T. Nagel, "Combustion Noise Investigation Final Report," FAA Report No. FAA-RD-77-3, 1977.

7. Pickett, G. F., "Turbine Noise Due to Turbulence and Temperature Fluctuation," Presented at the 8th International Congress on Acoustics, London, 1974.

8. Muthukrishnan, M., W. C. Strahle, and D. H. Neale, "Experimental and Analytical Separation of Hydrodynamic, Entropy and Direct Combustion Noise in a Gas Turbine Combustor," AIAA Paper 77-1275, 1977.

9. Motsinger, R. E., and J. J. Emmerling, "Review of Theory and Methods for Combustion Noise Prediction," AIAA Paper 75-541, 1975.

10. Mathews, D. C., and M. F. Rekos, Jr., "Direct Combustion Generated Noise in Turbopropulsion Systems-Prediction and Measurement," AIAA Paper 76-579, 1976.

11. Smith, T. B. J., and K. K. Kilham, "Noise Generation by Open Turbulent Flames," Journal of the Acoustical Society of America, Vol. 35, No. 5, 1963, pp. 715-724.

12. Knott, P. R., "Noise Generated by Turbulent Non-Premixed Flames," AIAA Paper 71-732, 1971.

13. Shivashankara, B. N., W. C. Strahle, and J. C. Handley, "Combustion Noise Radiation by Open Turbulent Flames," AIAA Paper 73-1025, 1973.

14. Strahle, W. C., and B. N. Shivashankara, "Combustion Generated Noise in Gas Turbine Combustors," Transactions of the ASME, April, 1976, pp. 242-246.

15. Shivashankara, B. N., and Robert W. Crouch, "Combustion Noise Characteristics of a Can-Type Combustor," AIAA Paper 76-578, 1976.

16. Mathews, D. C., and M. F. Rekos, Jr., "Prediction and Measurement of Direct Combustion Noise in Turbopropulsion Systems," Journal of Aircraft, Vol. 14, No. 9, 1977, pp. 850-859.

17. Strahle, W. C., and M. Muthukrishnan, "Correlation of Combustor Rig Sound Power Data and Theoretical Basis of Results," AIAA Journal, Vol. 18, No. 3, 1980, pp. 269-274.

18. Shivashankara, B. N., "Gas Turbine Core Noise Source Isolation by Internal-to-Far-Field Correlations," Journal of Aircraft, Vol. 15, No. 9, 1978, pp. 597-600.

19. Strahle, W. C., M. Muthukrishnan, and D. H. Neale, "Experimental and Analytical Separation of Hydrodynamic, Entropy and Direct Combustion Noise in a Gas Turbine Combustor," AIAA Paper 77-1275, 1977.

20. Miles, J. H., "Analysis of Pressure Spectra Measurements in a Ducted Combustion System," NASA Technical Memorandum 81583, 1981.

21. Strahle, W. C., "Combustion Noise," Prog. Energy Combustion Science, Vol. 4, 1978, pp. 157-176.

22. Legendre, R., "Bruit de combustion," La Recherche Aérospatiale, No. 5 (September-October), 1980, pp. 360-371.

23. Ho, P. Y., and V. L. Doyle, "Combustion Noise Prediction Up-Date," AIAA Paper 79-0588, 1979.

24. Muthukrishnan, M., W. C. Strahle, and D. H. Neale, "Estimation of Noise Source Strengths in a Gas Turbine Combustor," AIAA Paper 80-0034, 1980.

25. Levine, H., and J. Schwinger, "On the Radiation of Sound from an Unflanged Circular Pipe," Physical Review, Vol. 73, 1948, p. 383.

26. Ando, Y., "On the Sound Radiation from Semi-Infinite Circular Pipe of Certain Wall Thickness," Acustica, Vol. 22, 1969-70, p. 219.

27. Fricker, N., and C. A. Roberts, "The Measurement of the Acoustic Radiation Impedance of the Open End of a Thick Walled Tube with Hot Flow," Acustica, Vol. 37, No. 5, 1977.

28. Cummings, A., "High Temperature Effects on the Radiation Impedance of an Unflanged Duct Exit," Journal of Sound and Vibration, Vol. 52, No. 2, 1977, p. 299.

29. Cline, J. G., The Effects of Nonisentropic Flow on the Acoustic Response and Radiation Impedance of an Unflanged Circular Tube, Masters Thesis, Virginia Polytechnic Institute, March, 1980.

30. Zorumski, William E., "Generalized Radiation Impedance and Reflection Coefficients of Circular and Annular Ducts," Journal of the Acoustical Society of America, Vol. 54, No. 6, 1973, pp. 1667-1673.

31. Morse, P. M., Vibration and Sound, McGraw-Hill, New York, 1948, 2nd ed.

32. Johnston, G. W., and K. Ogimoto, "Sound Radiation from a Finite Length Unflanged Circular Duct with Uniform Axial Flow, I. Theoretical Analysis," Journal of the Acoustical Society of America, Vol. 68, 1980, pp. 1858-1870.

33. Johnston, G. W., and K. Ogimoto, "Sound Radiation from a Finite Length Unflanged Circular Duct with Uniform Axial Flow, II. Computed Radiation Characteristics," Journal of the Acoustical Society of America, Vol. 68, 1980, pp. 1871-1883.

34. Kinsler, L. E., and A. R. Frey, Fundamentals of Acoustics, John Wiley and Sons, New York, 1962.

35. Krejsa, E. A., Personal Communication, NASA Lewis Research Center, 8 July 1982.

36. Mahan, J. R., and J. M. Kasper, "Influence of Heat Release Distribution on the Acoustic Response of Long Burners," ASME Paper 79-DET-31, September 1979.

37. VanWylen, G. J., and R. E. Sonntag, Fundamentals of Classical Thermodynamics, John Wiley and Sons, 1976, p. 683.

38. Lord Rayleigh, Theory of Sound, Vol. 2, Dover Publications, Second Edition, 1945.

39. Riley, J. F., R. G. Leonard, and V. W. Goldschmidt., A Transfer Function and Experimental Analysis of Feedback Excited Oscillations in Gas Flames, Purdue University Report No. 8 HL 74-29, 1974.

40. Pierce, A. D., Acoustics: An Introduction to its Physical Principles and Applications, McGraw-Hill, New York, 1981.

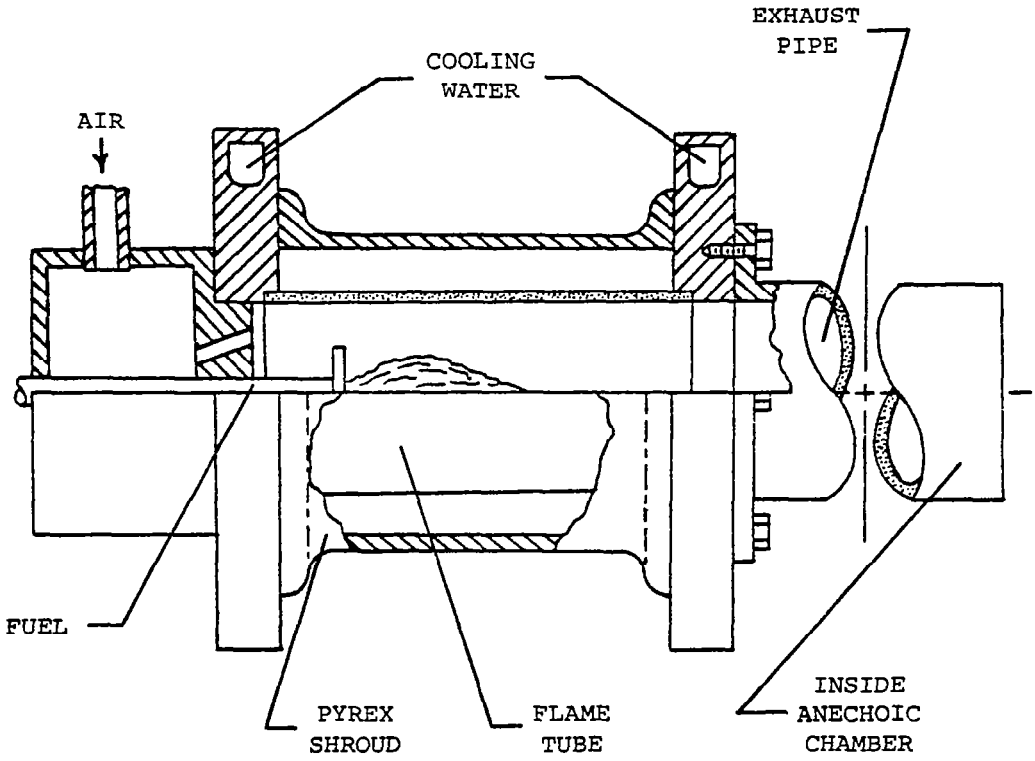

Fig. 1. Cut-Away View of Experimental Burner.

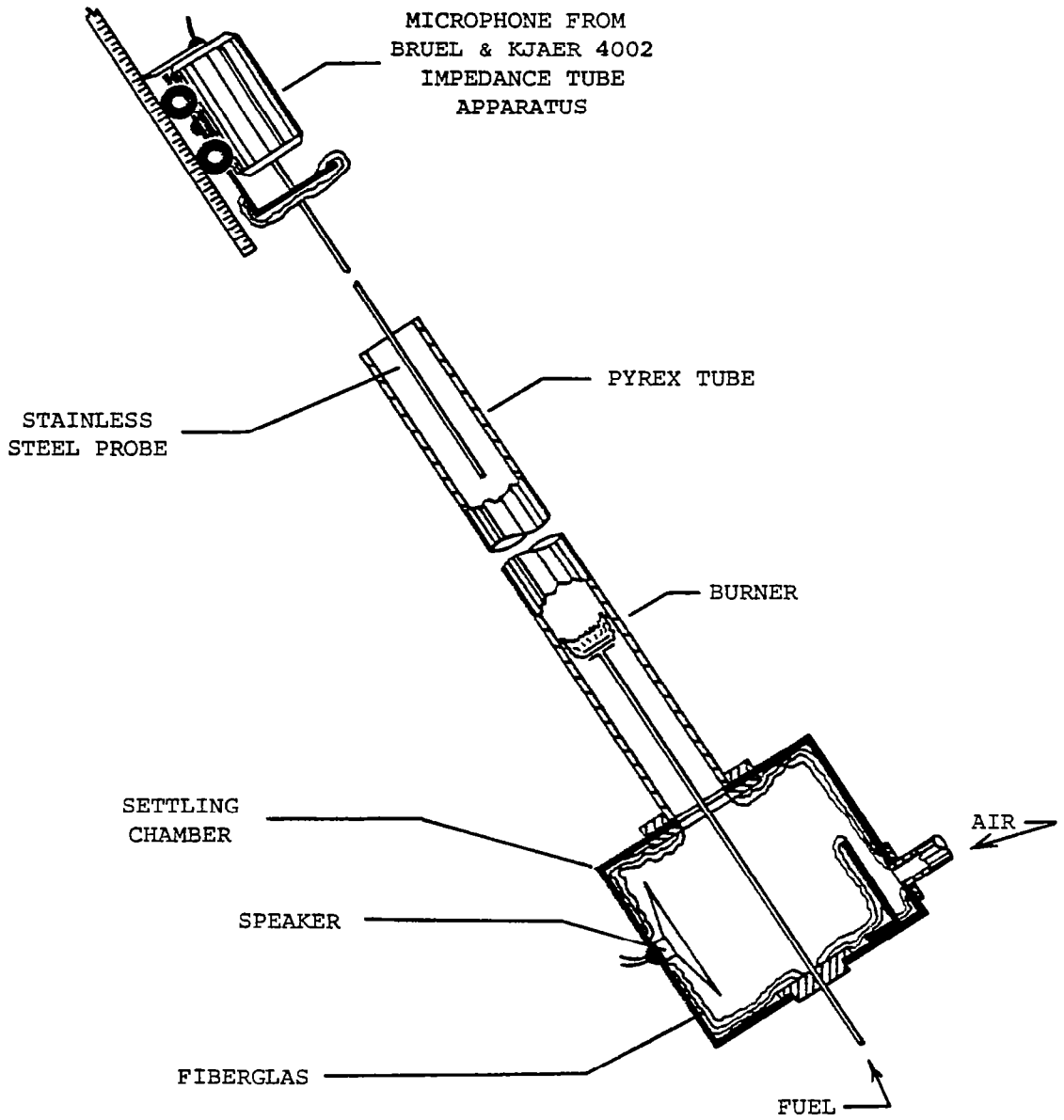

Fig. 2. Apparatus for the Preliminary Study.

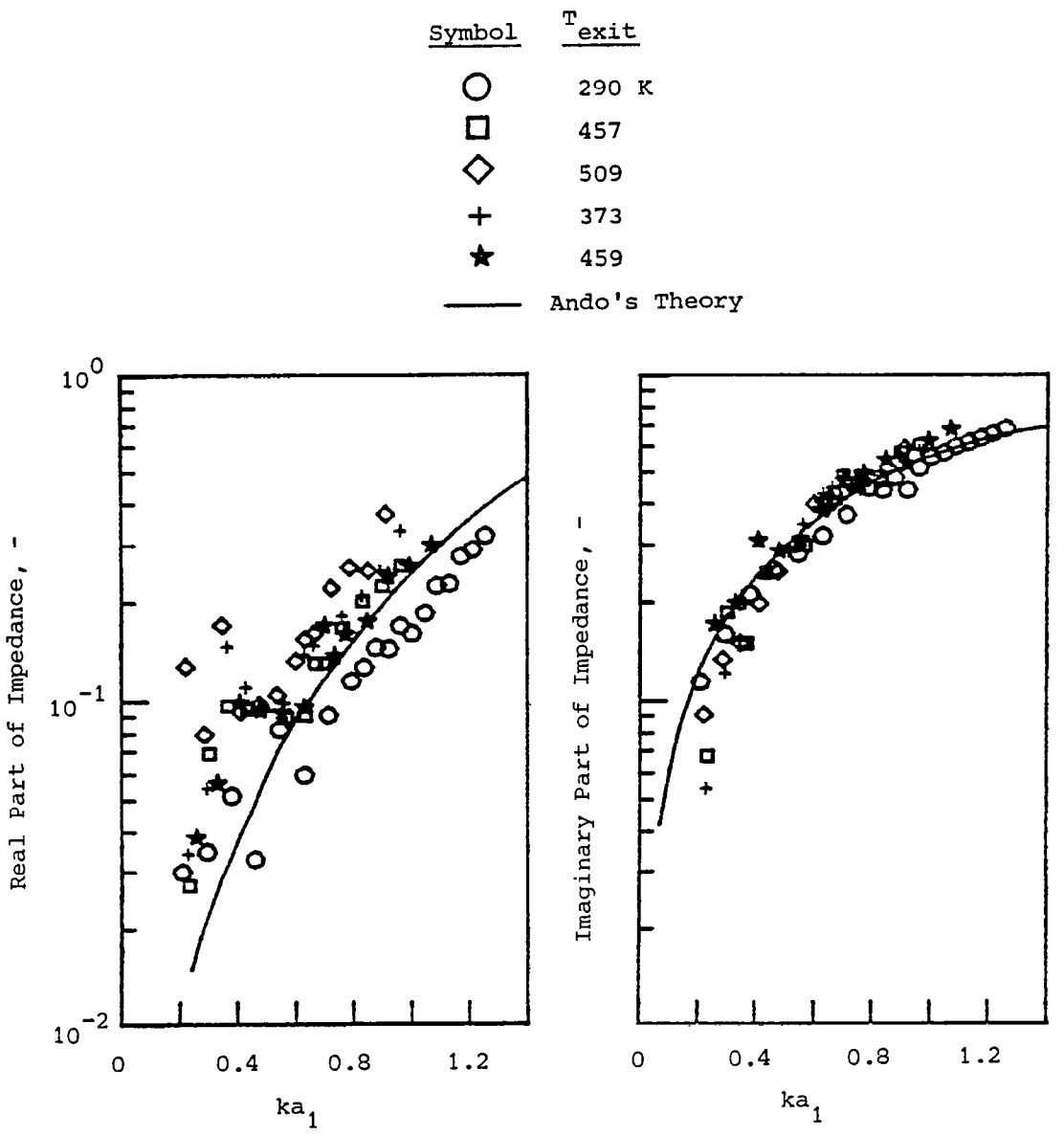

Fig. 3. Specific Radiation Impedance Measured at the Open End of a Circular Tube With the Flow of a Hot Gas Using the Classical Impedance Tube Method.

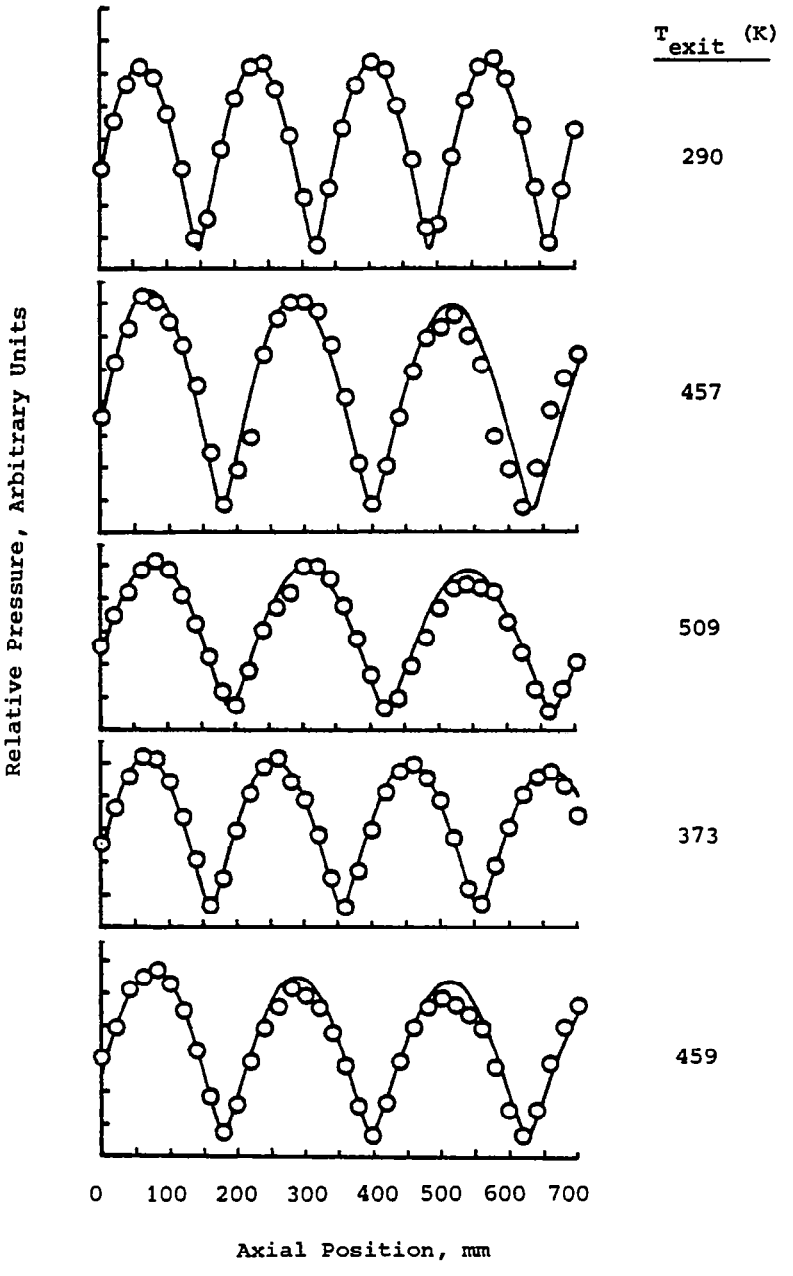

Fig. 4. Comparison of Measured and Computed Waveforms.

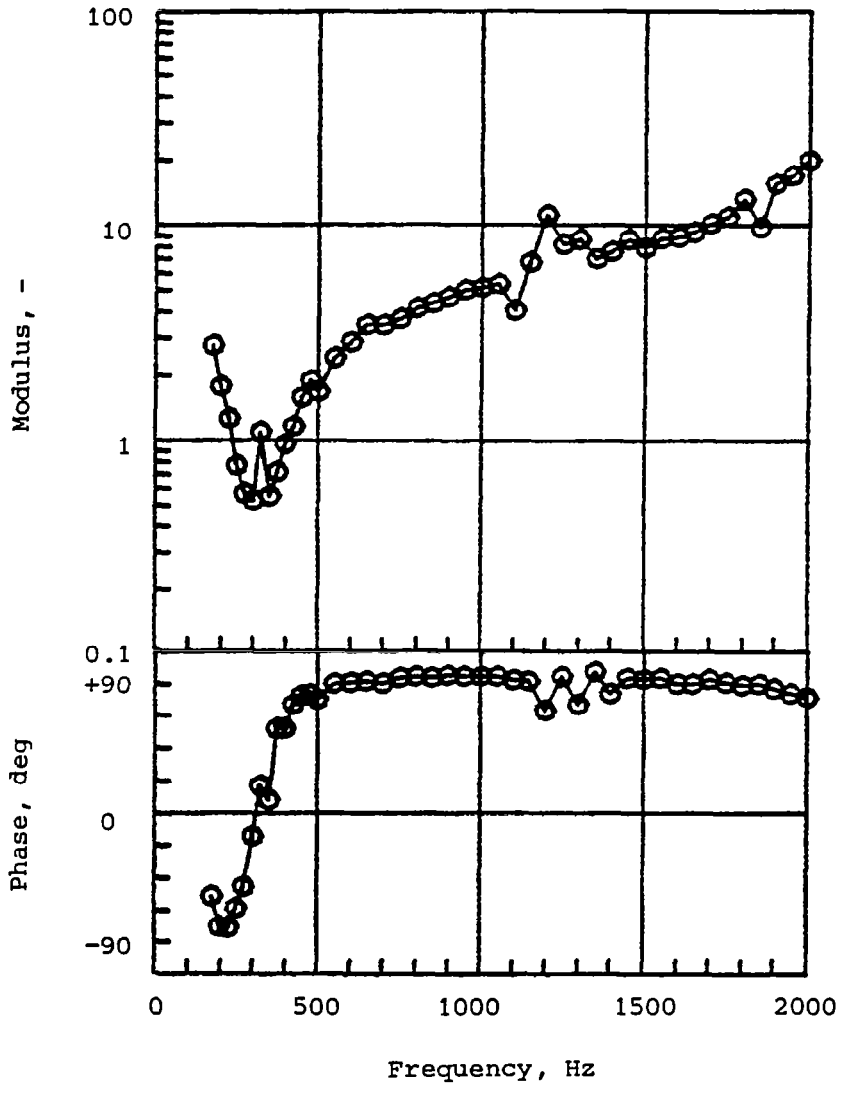

Fig. 5. Specific Impedance at Closed End of Burner.

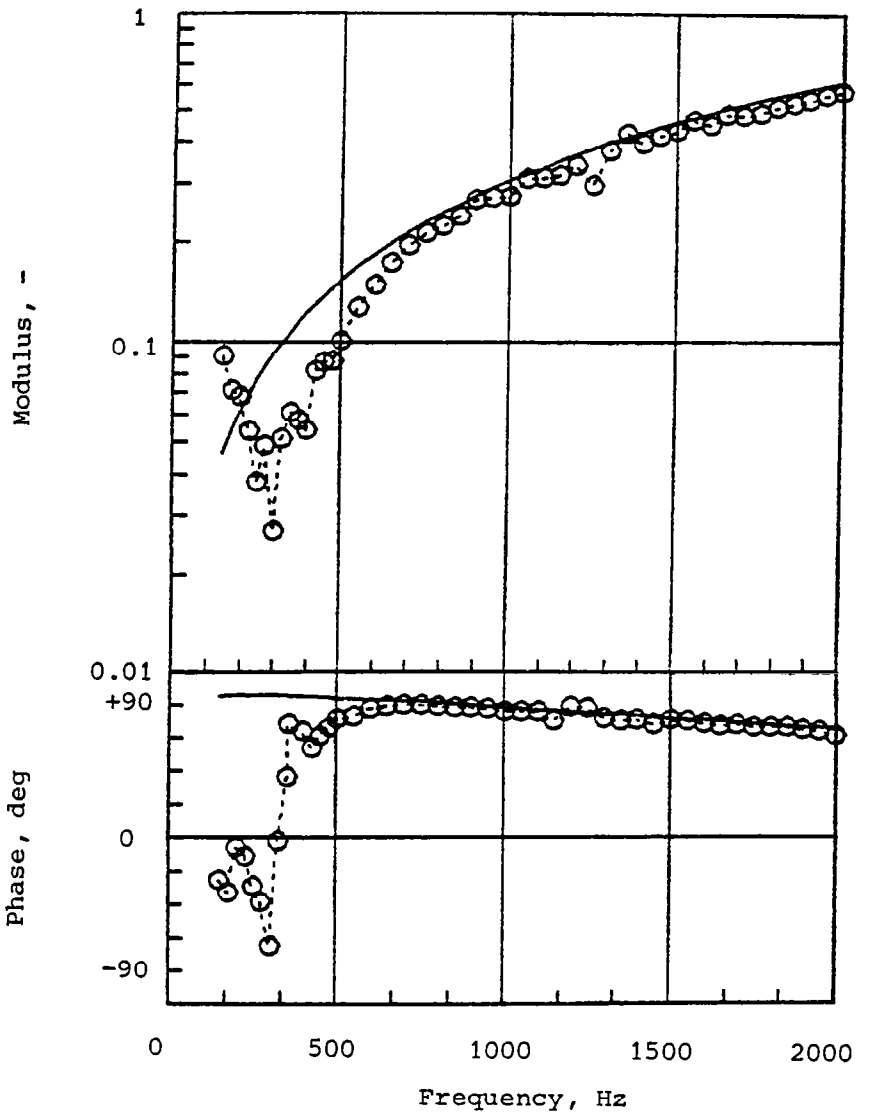

Fig. 6. Specific Impedance at Open End of Burner (Line is Ando's Theory).

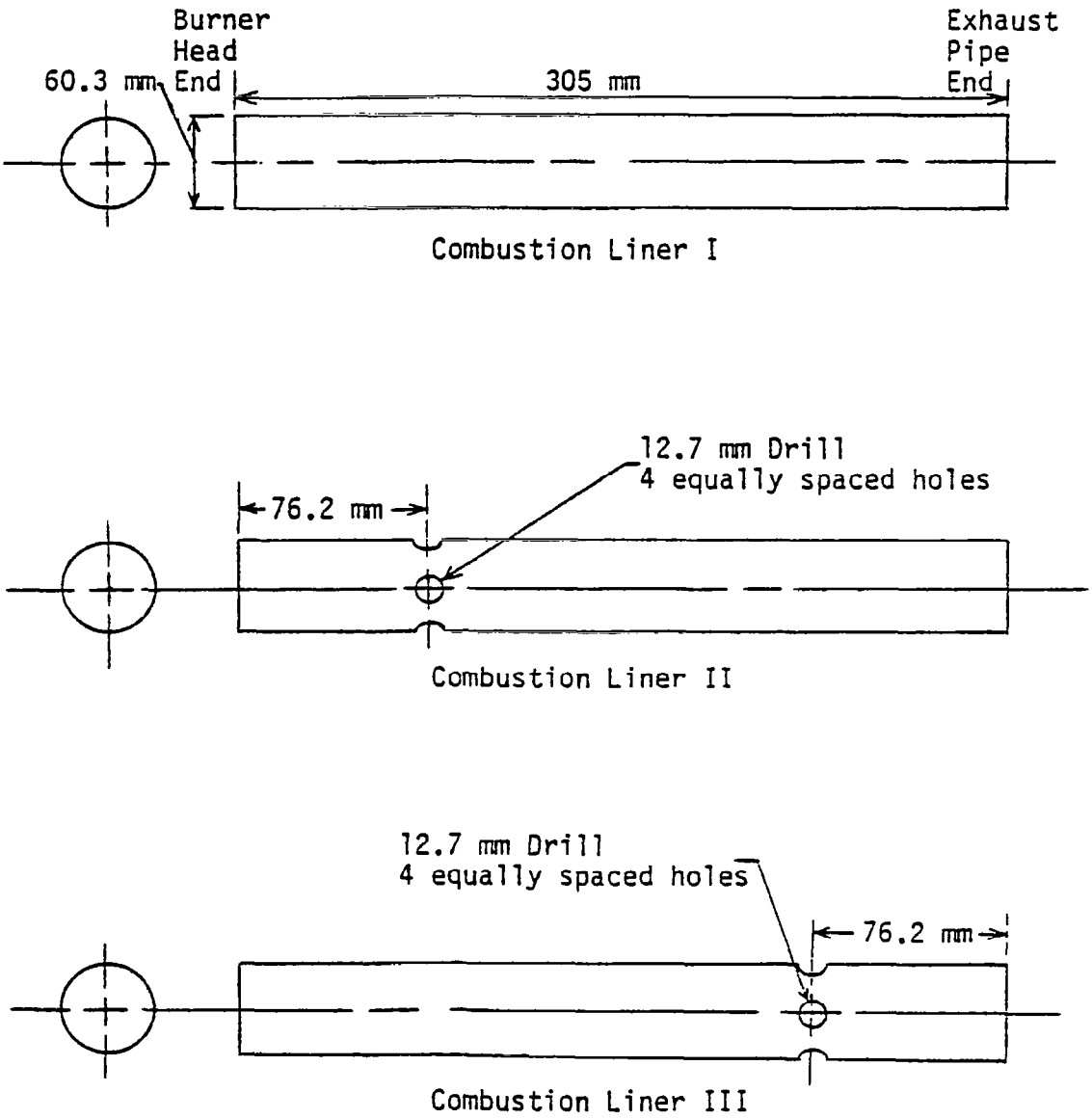

Fig. 7. Hole Patterns of Combustion Liners I, II and III.

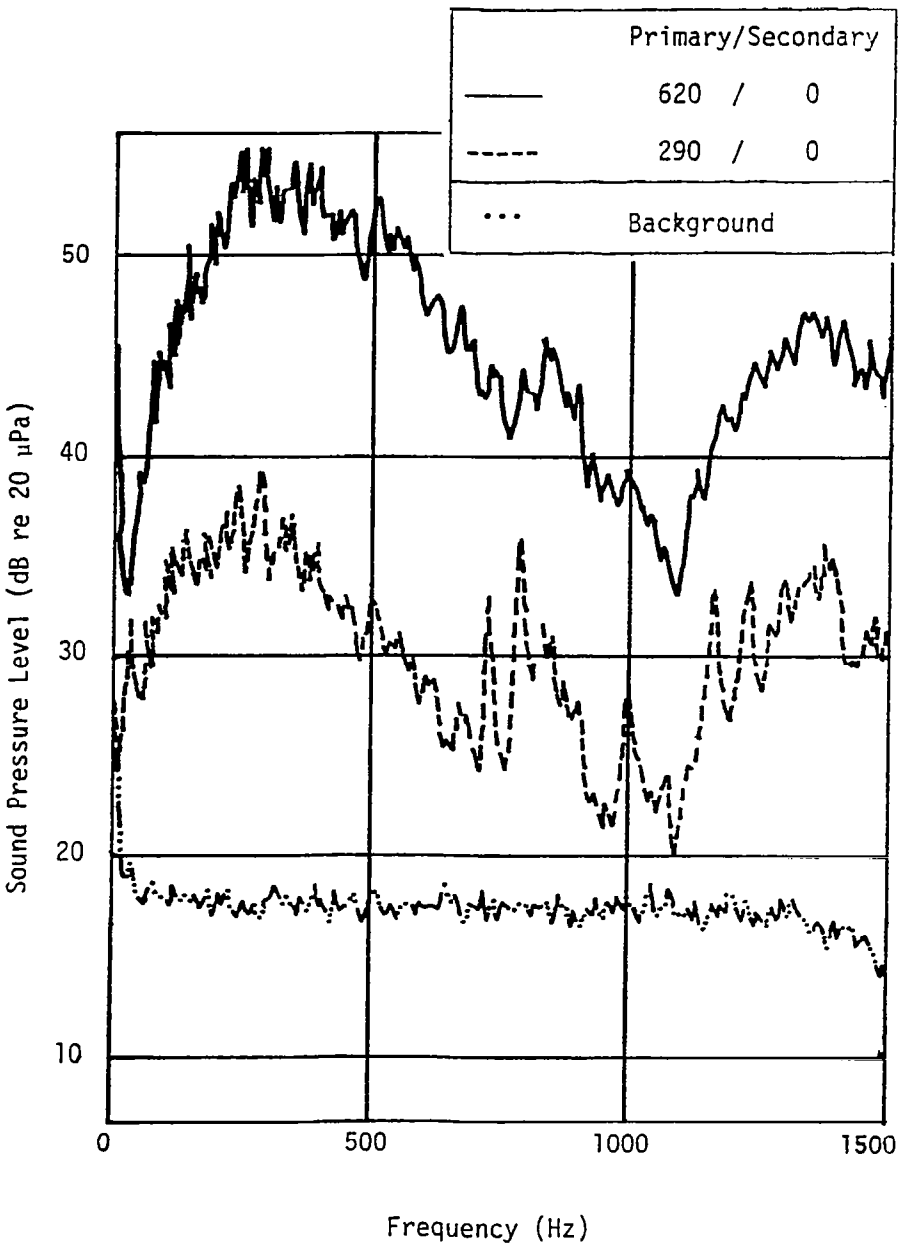

Fig. 8. Typical Background and Air Flow Noise for Liner I at On-Axis Microphone.

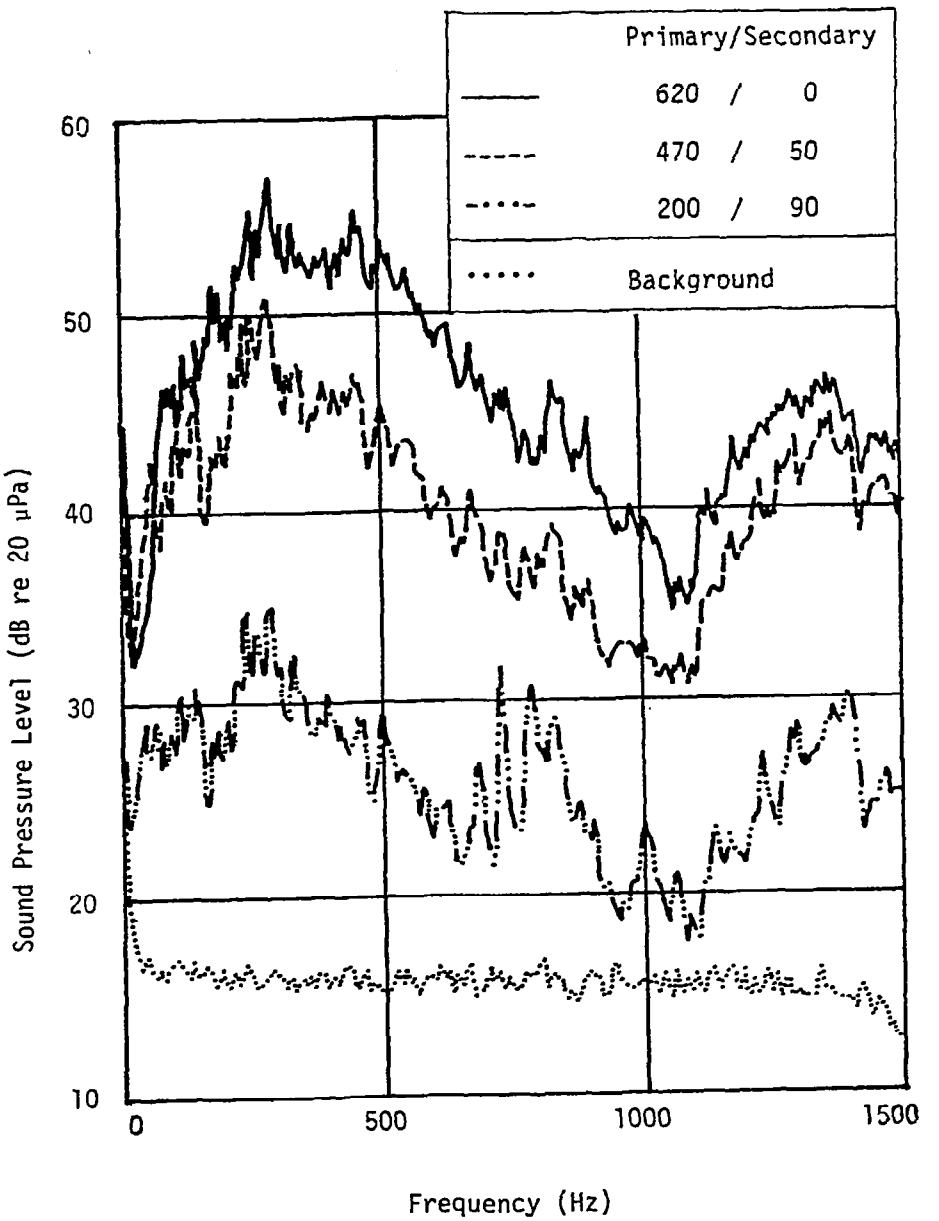

Fig. 9. Typical Background and Air Flow Noise for Liner II at On-Axis Microphone.

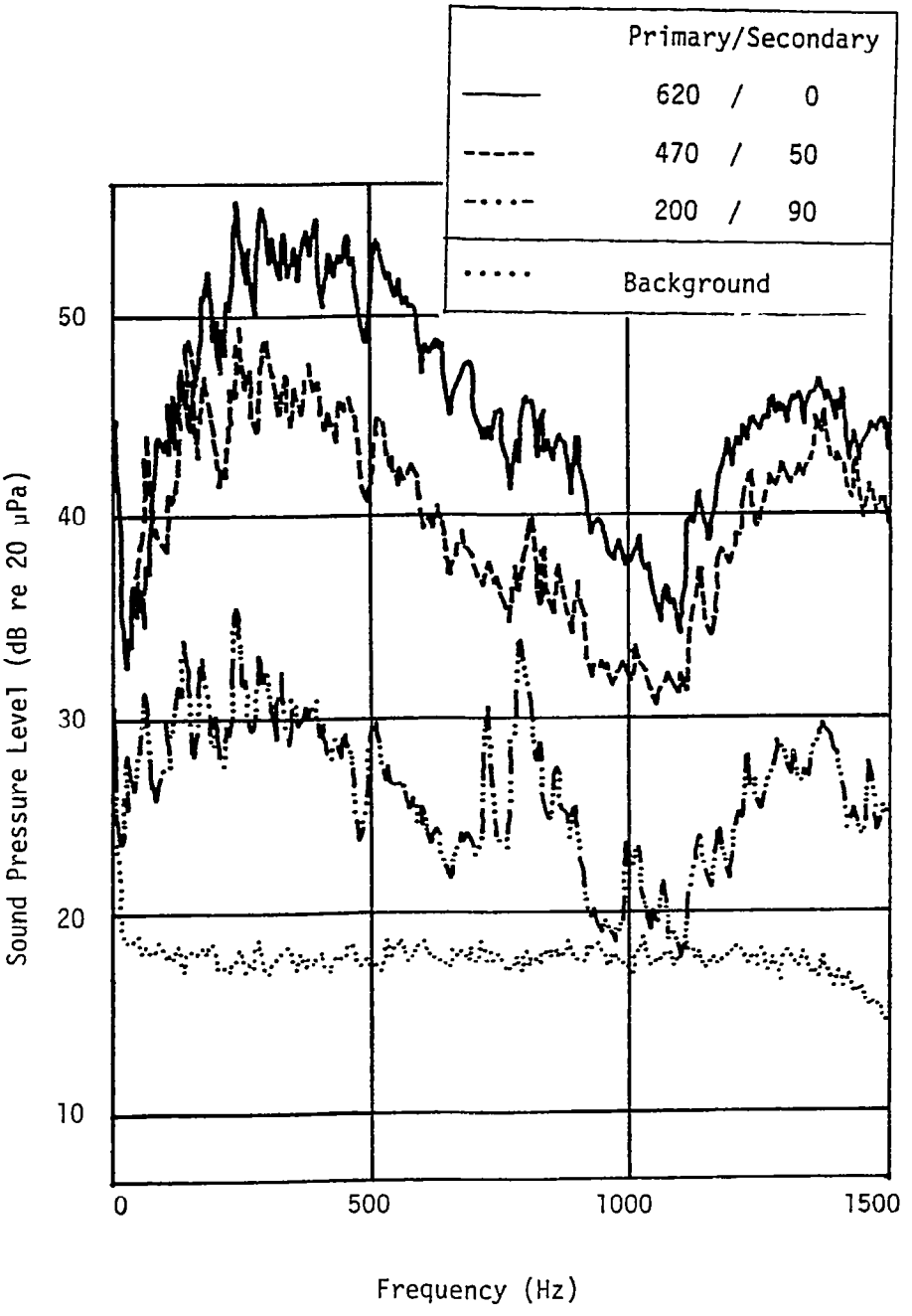

Fig. 10. Typical Background and Air Flow Noise for Liner III at On-Axis Microphone.

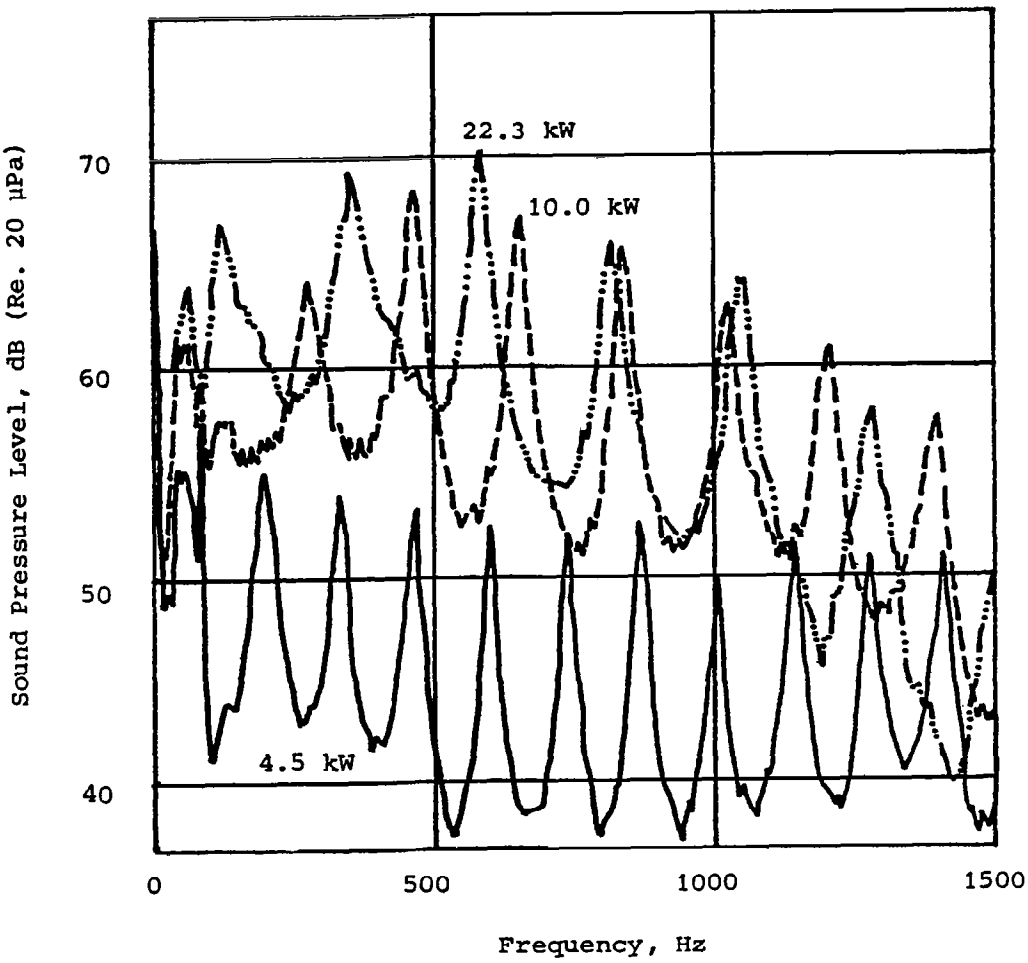

Fig. 11. Comparison of Sound Pressure Spectra for Combustion Liner I, Three Power Levels, (On-Axis Microphone).

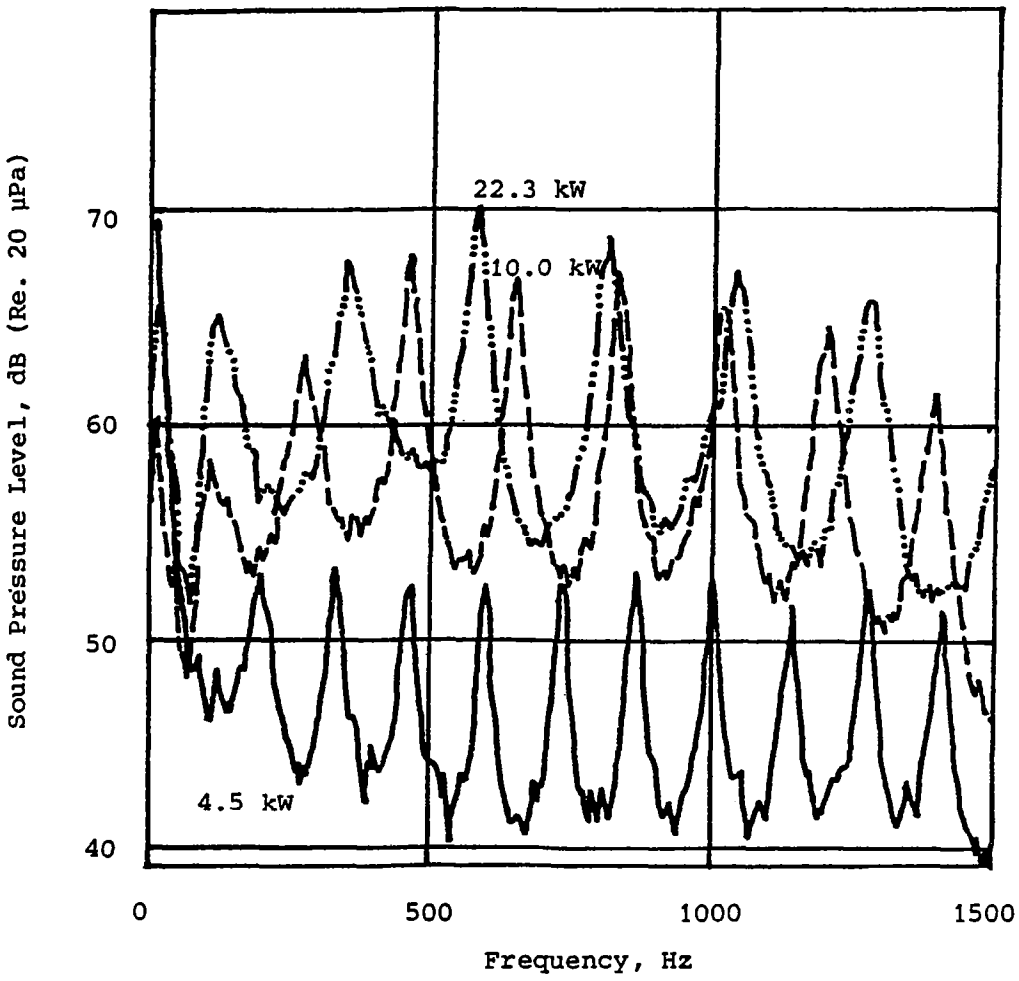

Fig. 12. Comparison of Sound Pressure Spectra for Combustion Liner I, Three Power Levels, (Off-Axis Microphone).

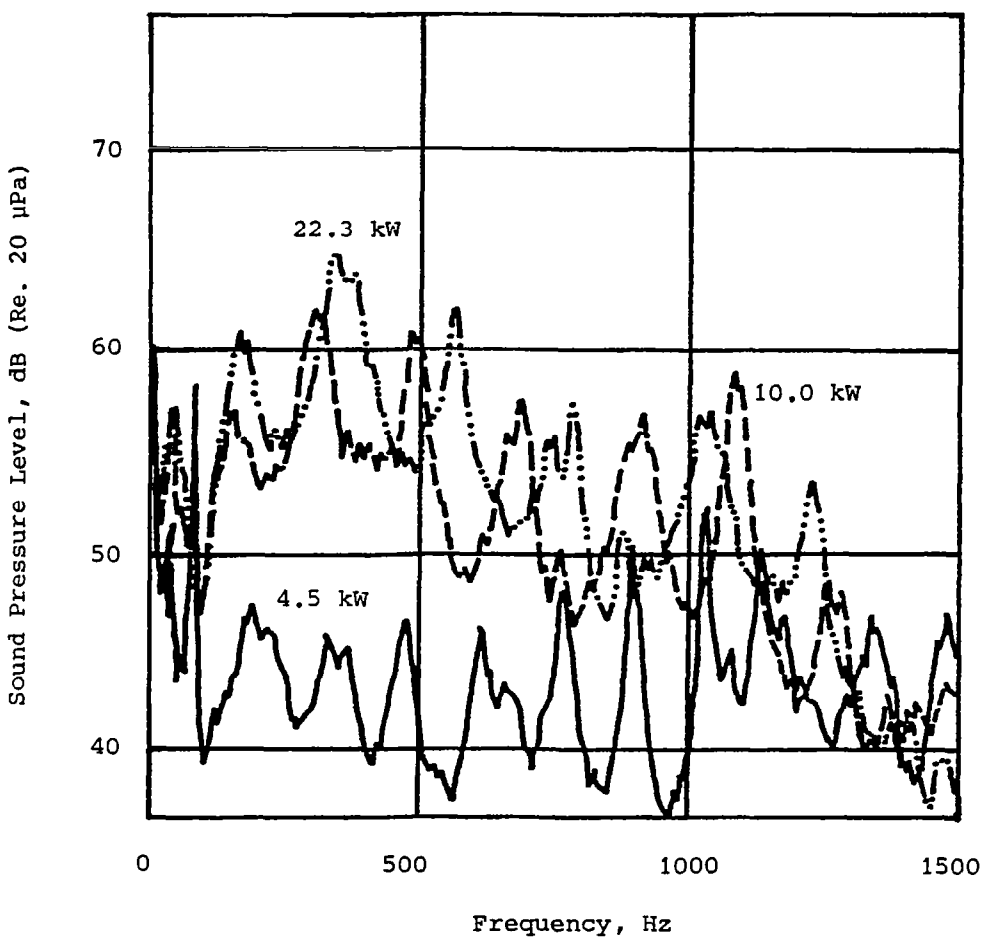

Fig. 13. Comparison of Sound Pressure Spectra for Combustion Liner II, Three Power Levels, (Primary Air Flow = 470 SLPM, Secondary Air Flow = 150 SLPM, On-Axis Microphone).

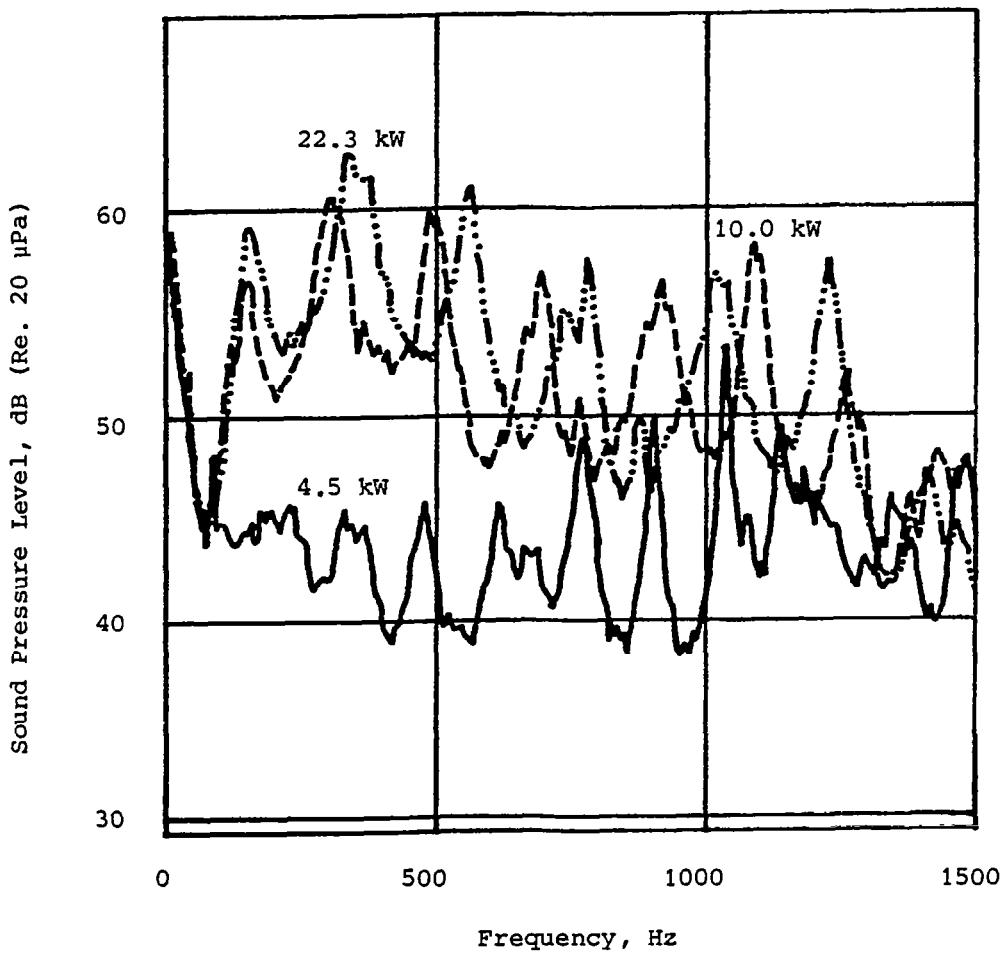

Fig. 14. Comparison of Sound Pressure Spectra for Combustion Liner II, Three Power Levels, (Primary Air Flow = 470 SLPM, Secondary Air Flow = 150 SLPM, Off-Axis Microphone).

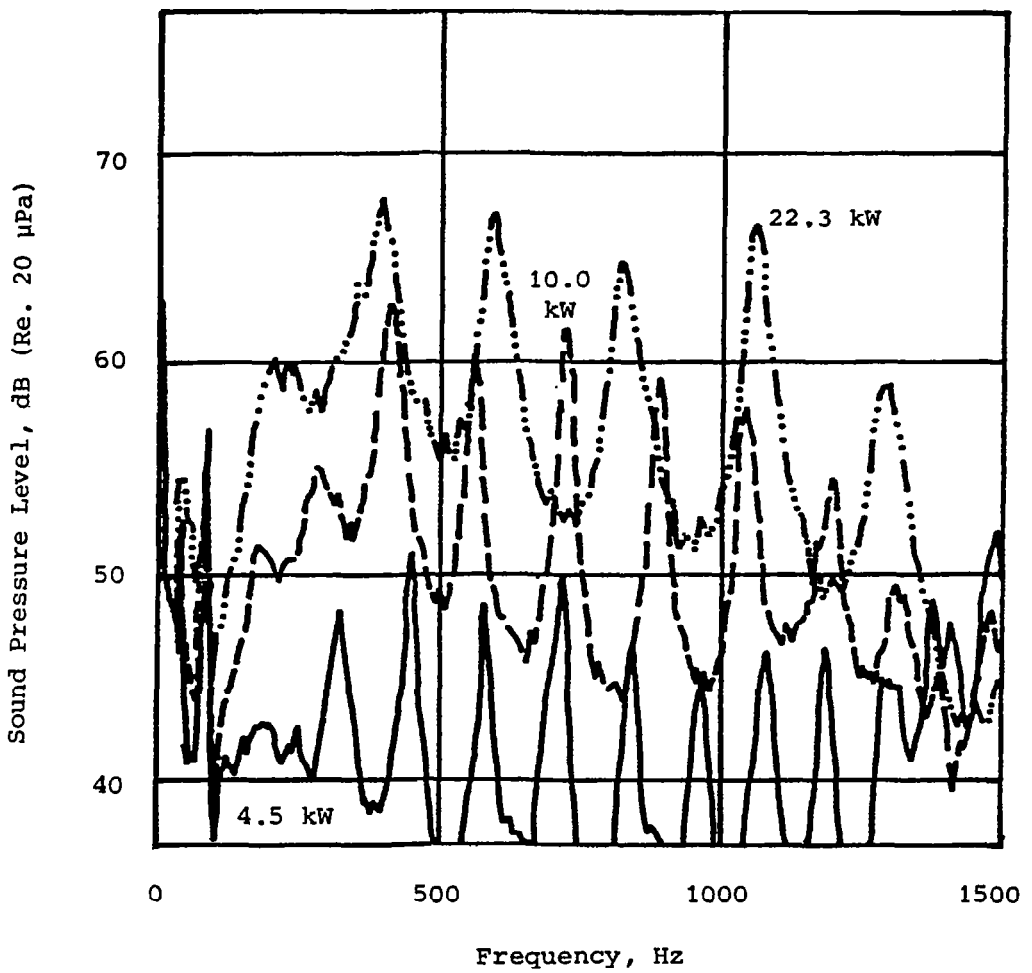

Fig. 15. Comparison of Sound Pressure Spectra for Combustion Liner III, Three Power Levels, (Primary Air Flow = 470 SLPM, Secondary Air Flow = 150 SLPM, On-Axis Microphone).

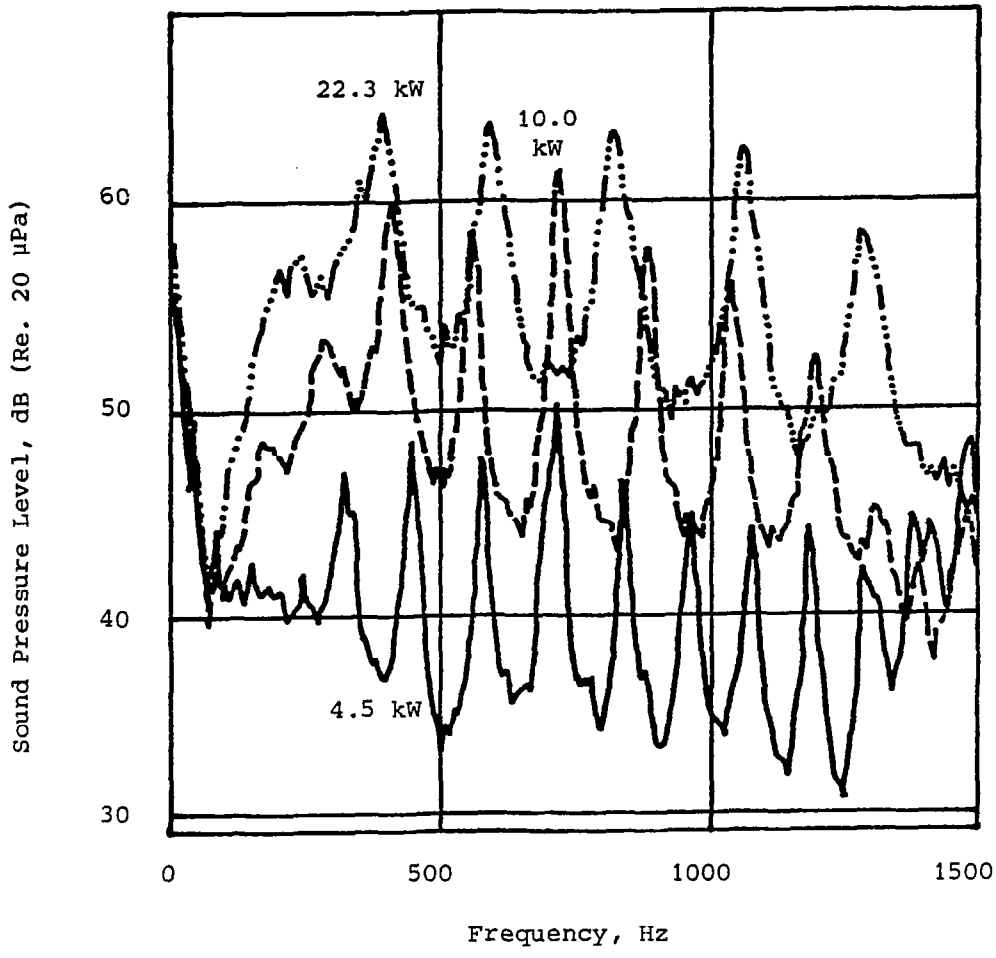

Fig. 16. Comparison of Sound Pressure Spectra for Combustion Liner III, Three Power Levels, (Primary Air Flow = 470 SLPM, Secondary Air Flow = 150 SLPM, Off-Axis Microphone).

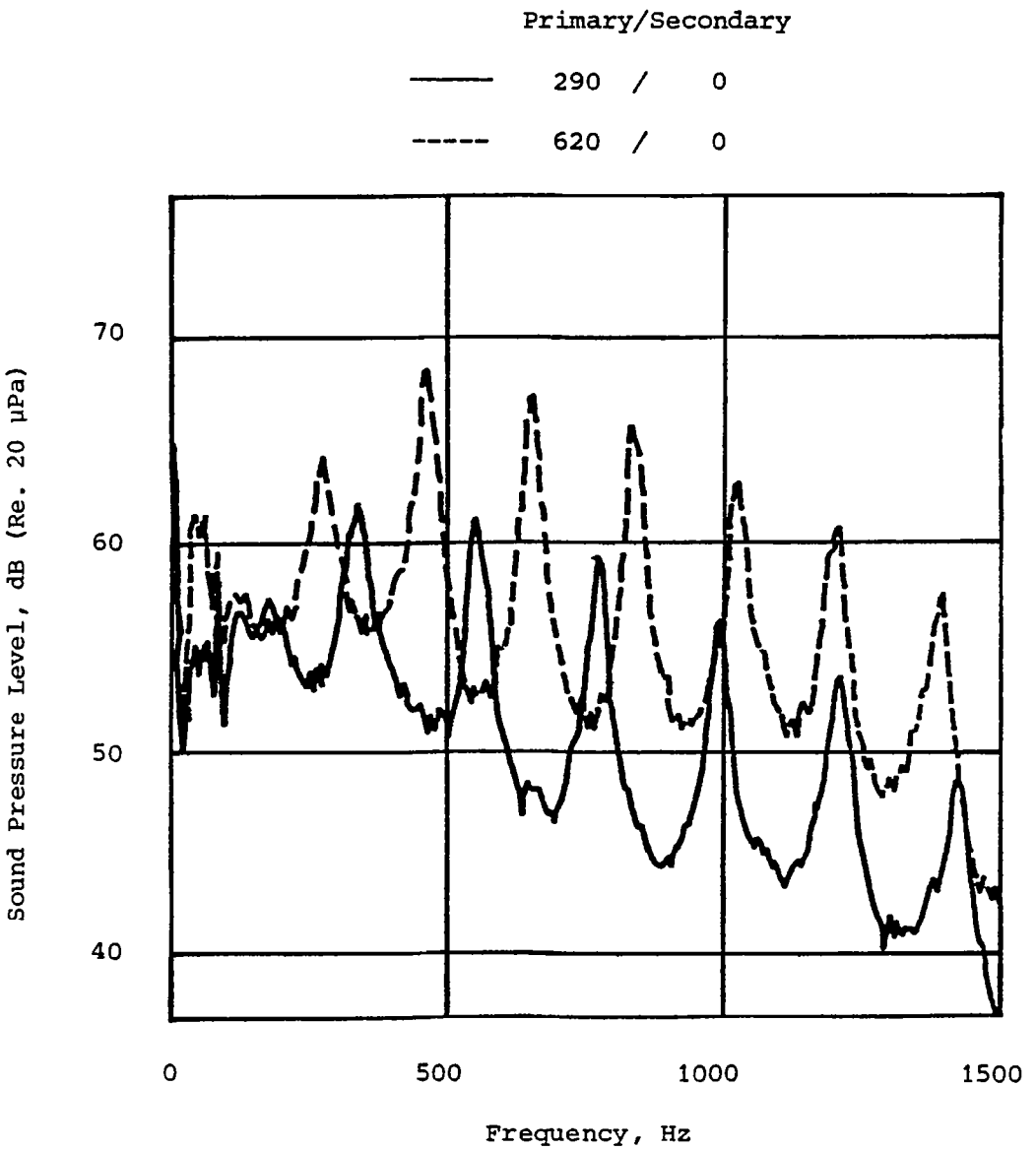

Fig. 17. Comparison of Sound Pressure Spectra for Two Air Flow Rates for Combustion Liner I.

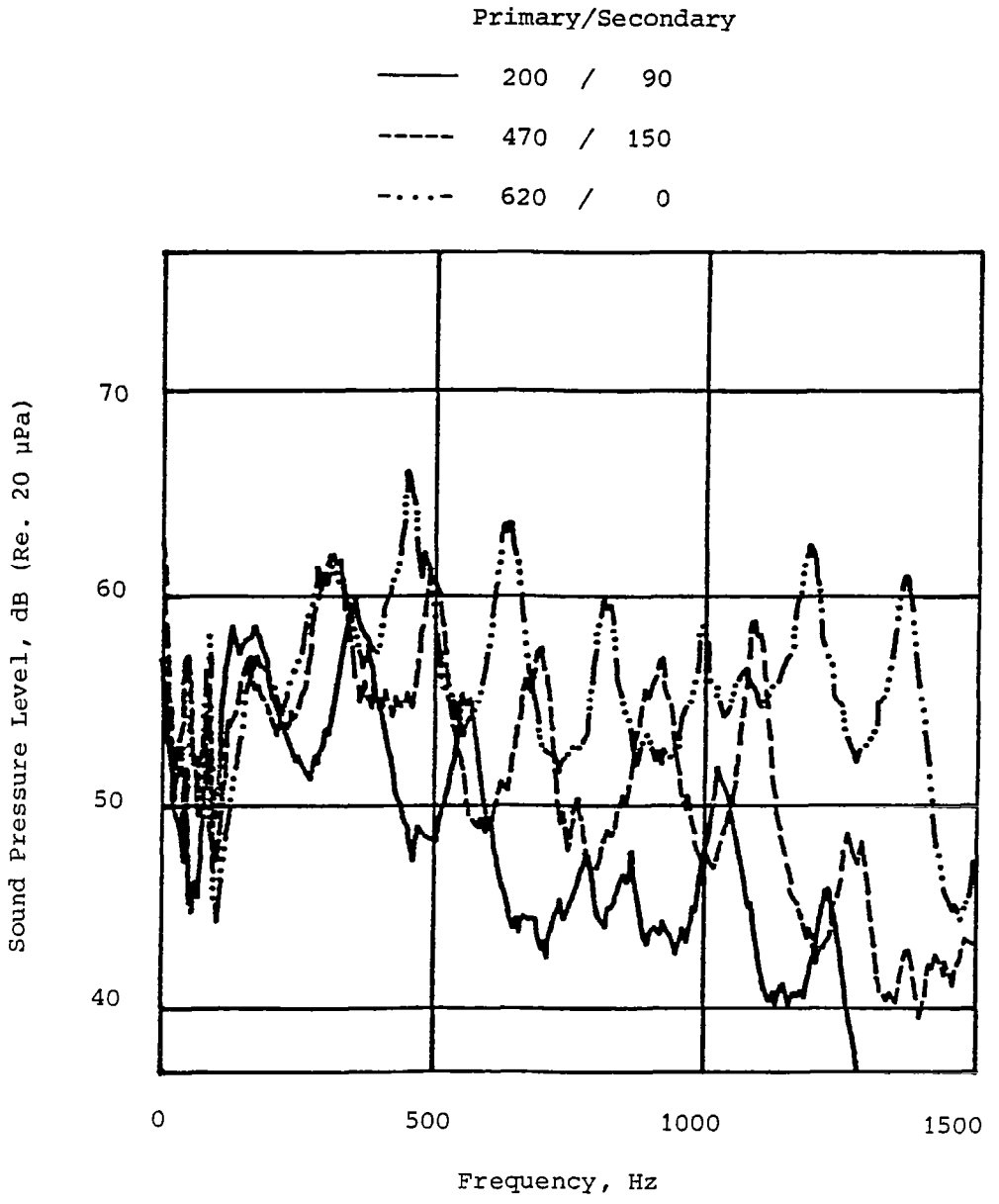

Fig. 18. Comparison of Sound Pressure Spectra for Three Air Flow Combinations for Liner II.

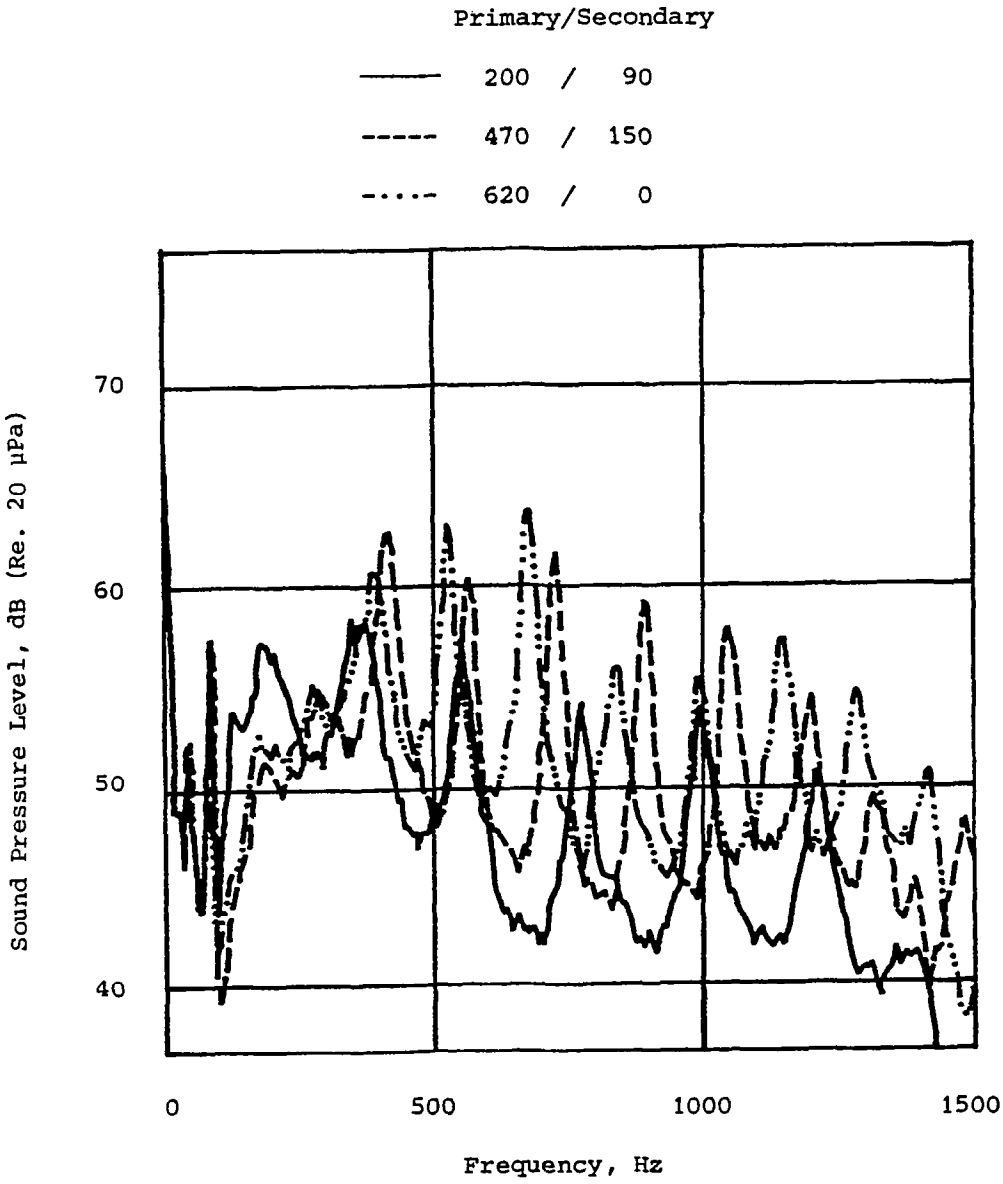

Fig. 19. Comparison of Sound Pressure Spectra for Three Air Flow Combinations for Liner III.

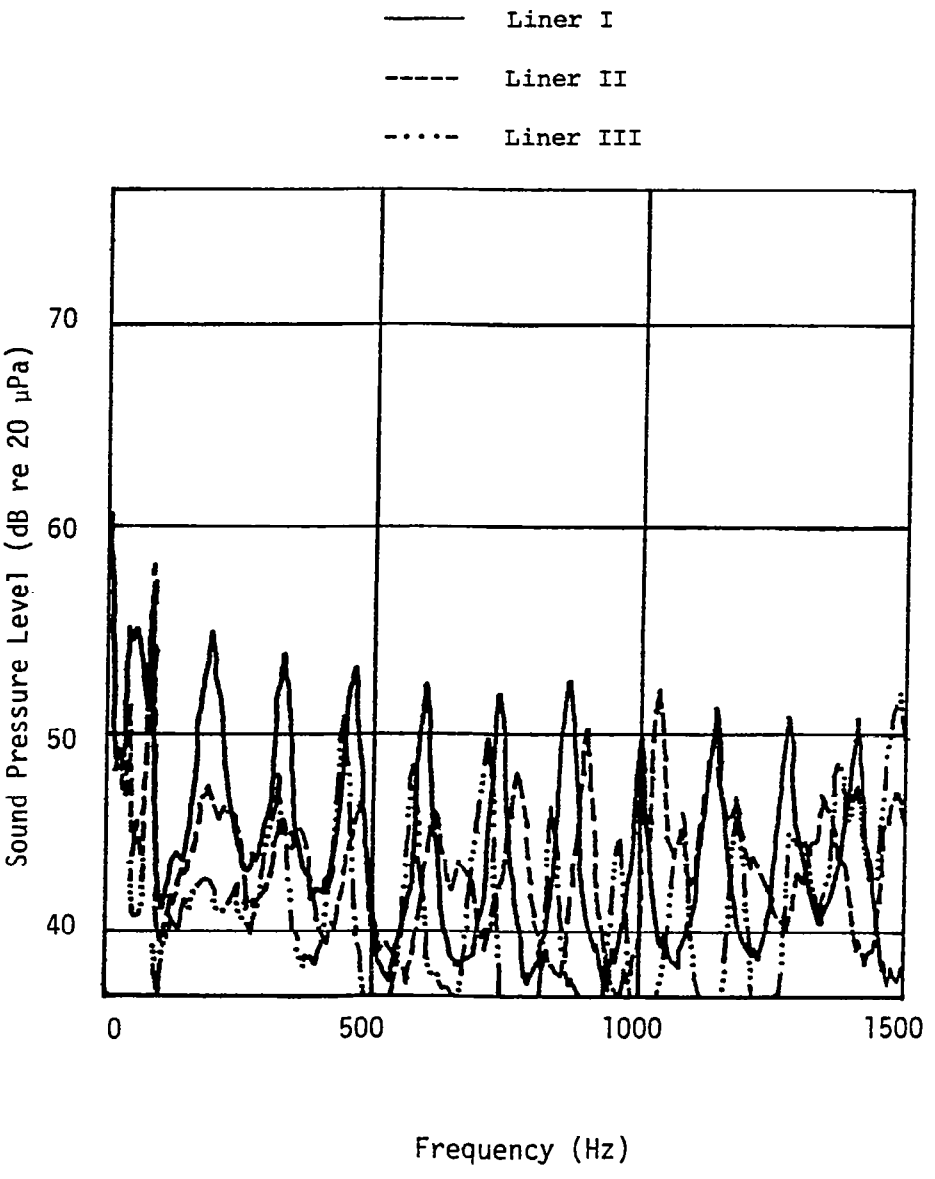

Fig. 20. Comparison of Sound Pressure Spectra for the Three Liners (4.5 kW, Total Air Flow = 620 SLPM).

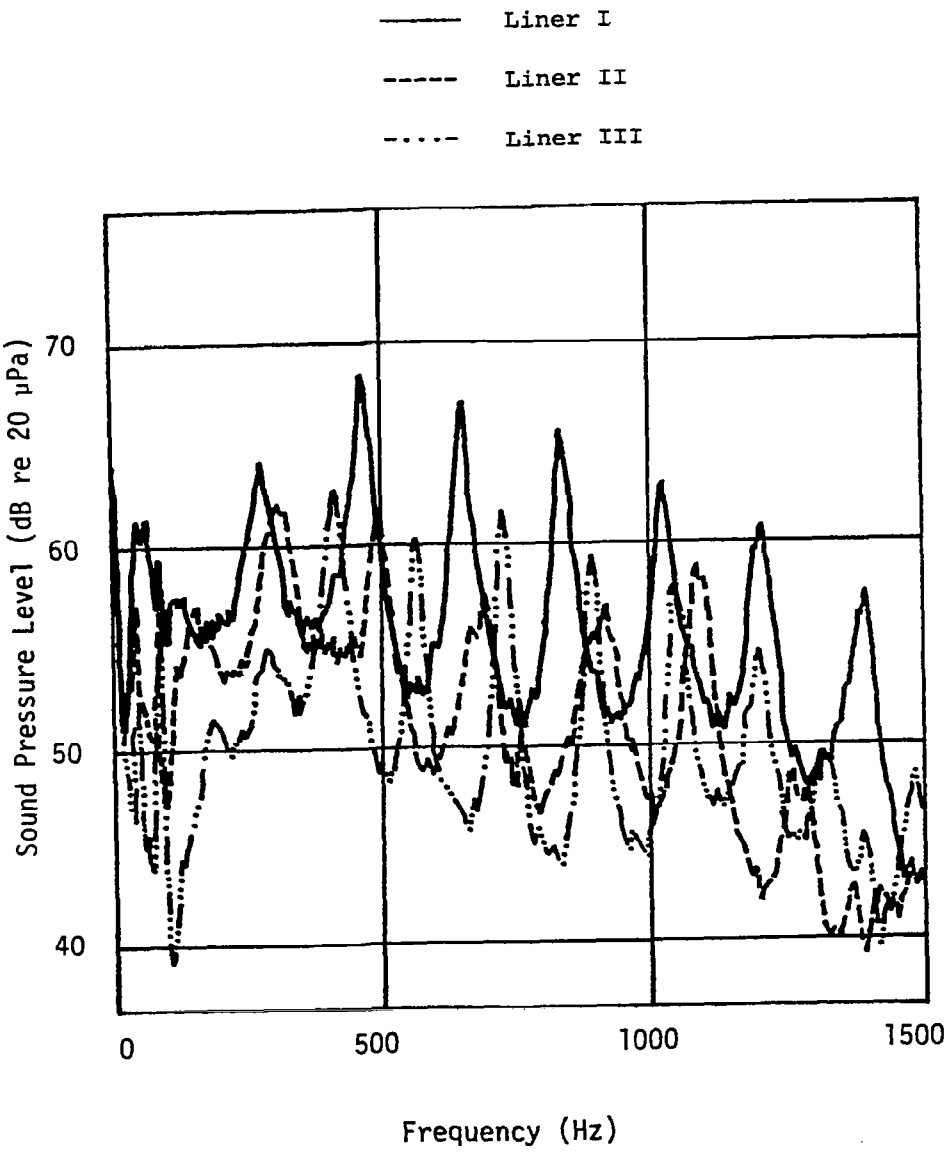

Fig. 21. Comparison of Sound Pressure Spectra for the Three Liners (10.0 kW, Total Air Flow = 620 SLPM).

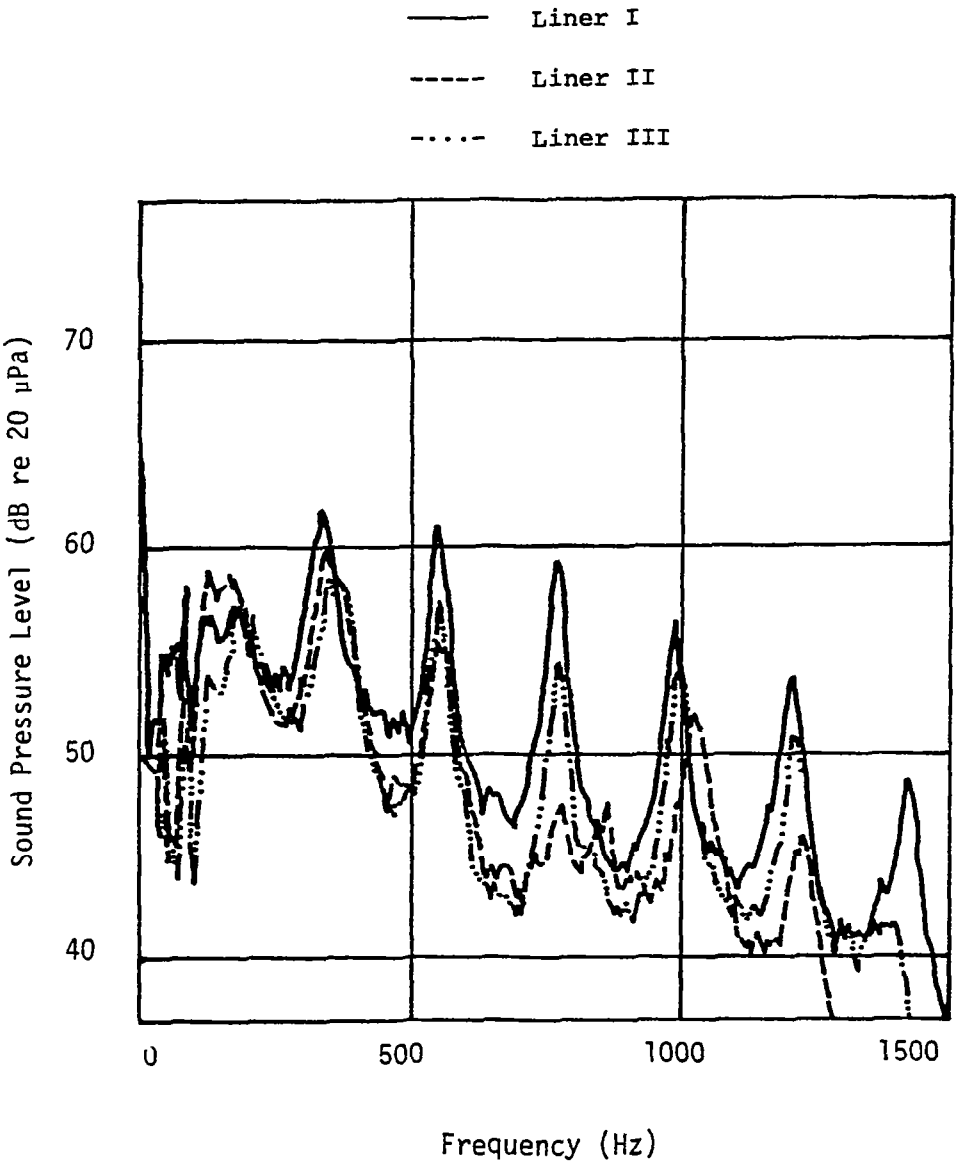

Fig. 22. Comparison of Sound Pressure Spectra for the Three Liners (22.3 kW, Total Air Flow = 290 SLPM).

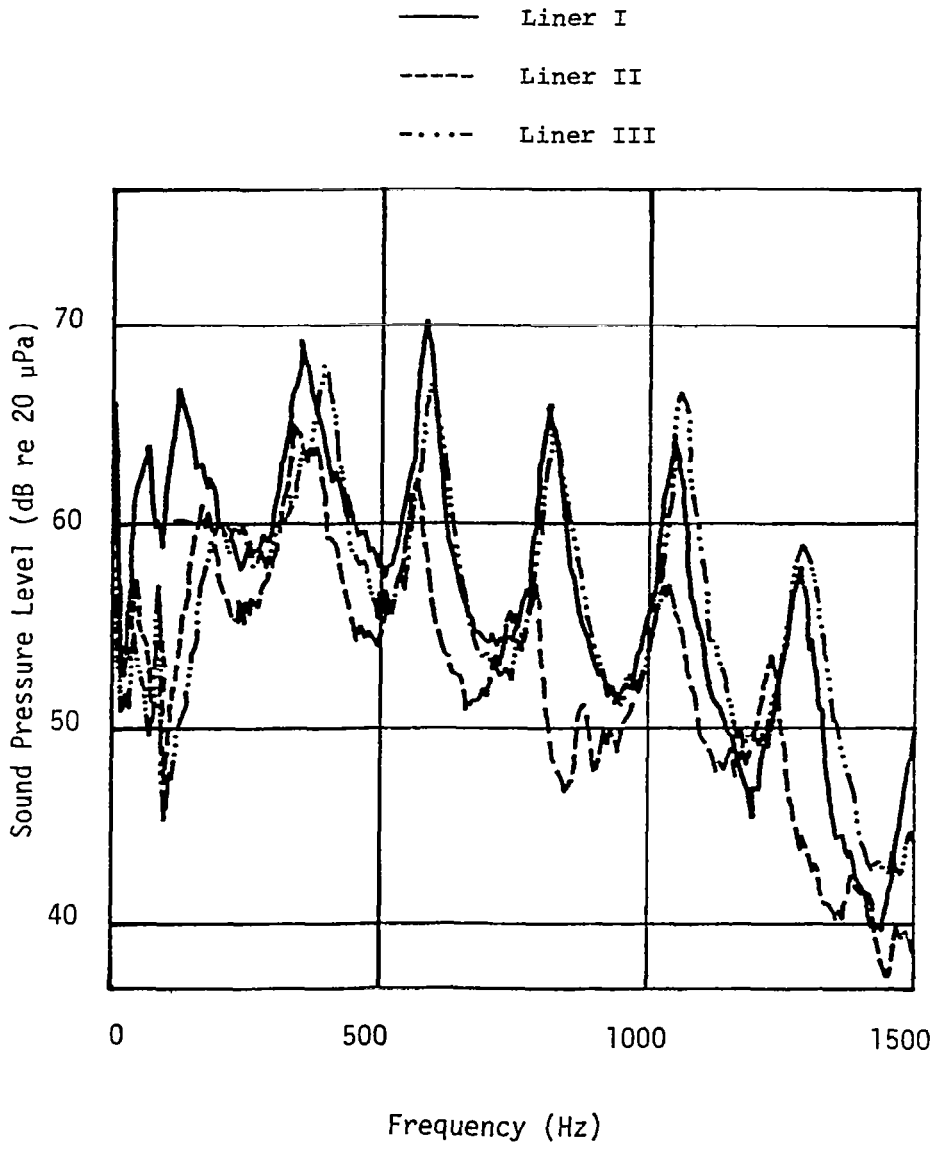

Fig. 23. Comparison of Sound Pressure Spectra for the Three Liners (22.3 kW, Total Air Flow = 620 SLPM).

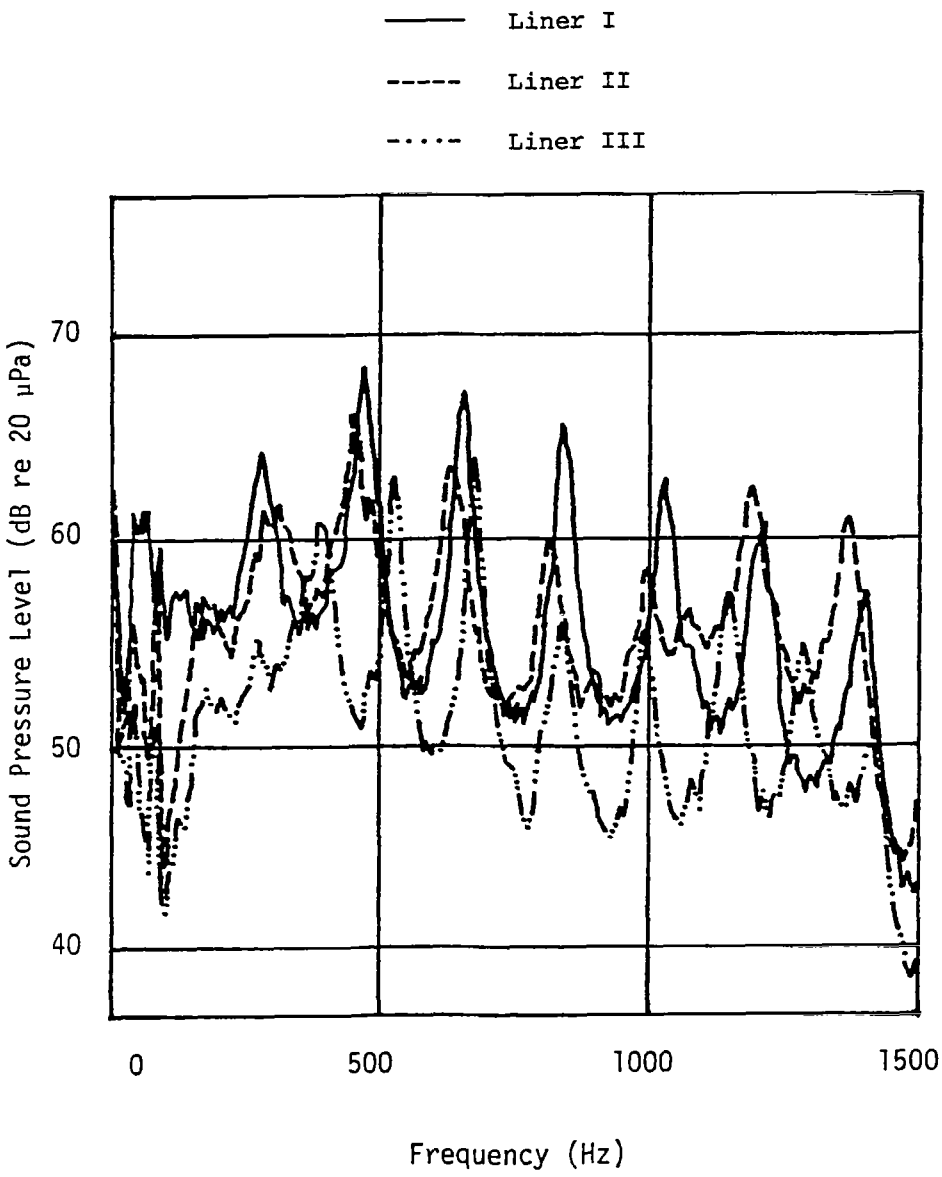

Fig. 24. Comparison of Sound Pressure Spectra for the Three Liners (10.0 kW, Primary Air Flow = 620 SLPM).

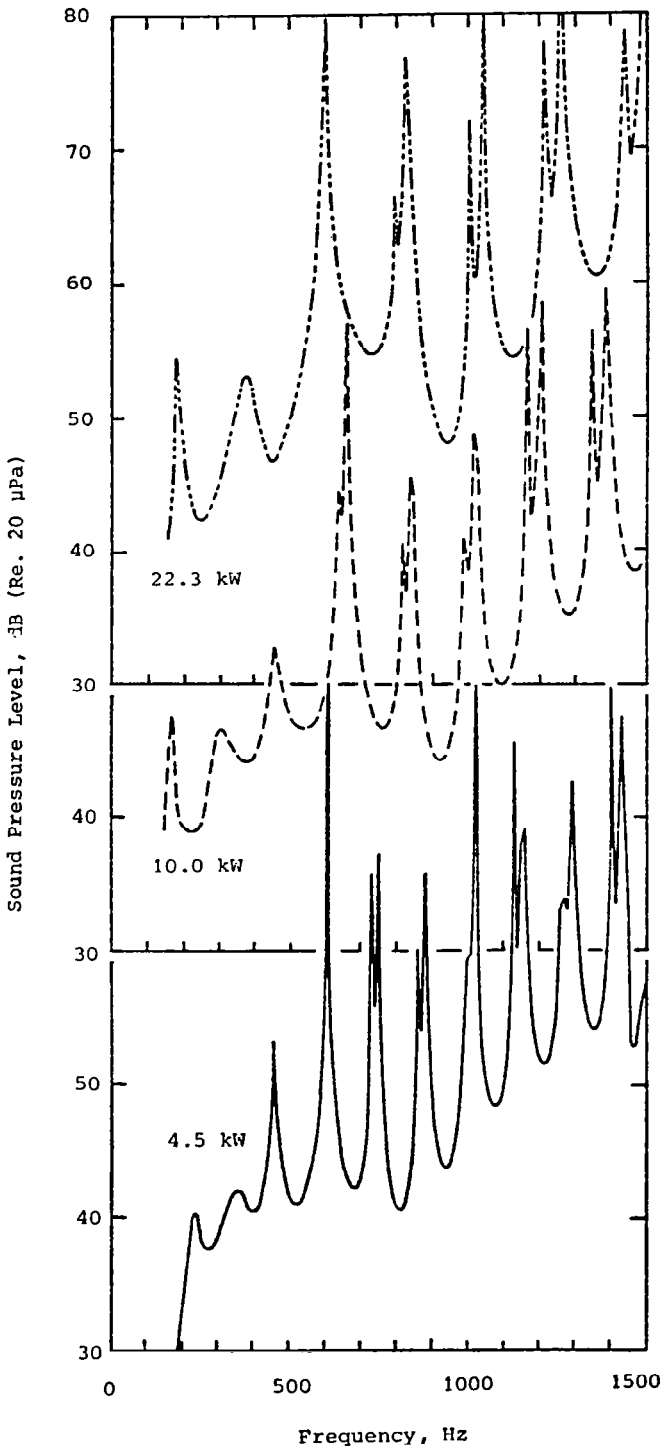

Fig. 25. Primitive Sound Spectra.

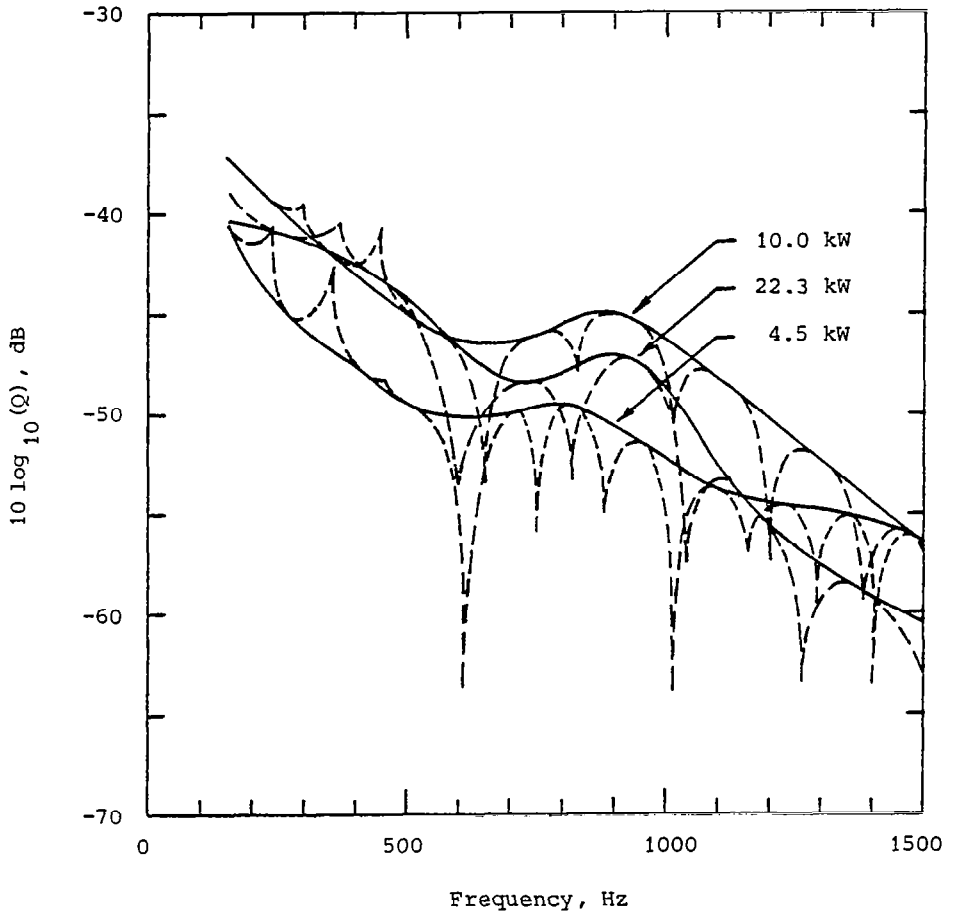

Fig. 26. The Thermal-Acoustic Efficiency Spectra Corresponding to the Sound Pressure Spectra of Fig. 11.

1. Report No.	2. Government Accession No.	3. Recipient's Catalog No.
NASA CR-3725		

4. Title and Subtitle

Experimental Study of the Thermal-Acoustic Efficiency in a Long Turbulent Diffusion-Flame Burner

5. Report Date

August 1983

6. Performing Organization Code

7. Author(s)

J. R. Mahan

8. Performing Organization Report No.

None

10. Work Unit No.

9. Performing Organization Name and Address

Virginia Polytechnic Institute and State University
Dept. of Mechanical Engineering
Blacksburg, Virginia 24061

11. Contract or Grant No.

NAG3-124

13. Type of Report and Period Covered

Contractor Report

12. Sponsoring Agency Name and Address

National Aeronautics and Space Administration
Washington, D.C. 20546

14. Sponsoring Agency Code

505-32-02 (E-1739)

15. Supplementary Notes

Final report. Project Manager, Eugene A. Krejsa, Fluid Mechanics and Instrumentation Division. NASA Lewis Research Center, Cleveland, Ohio 44135

16. Abstract

An acoustic source/propagation model is used to interpret measured noise spectra from a long turbulent burner. The acoustic model is based on the perturbation solution of the equations describing the unsteady one-dimensional flow of an inviscid ideal gas with a distributed heat source. The model assumes that the measured noise spectra are due uniquely to the unsteady component of combustion heat release. The model was applied to a long cylindrical hydrogen burner operating over a range of power levels between 4.5 kW and 22.3 kW. Acoustic impedances at the inlet to the burner and at the exit of the tube downstream of the burner were measured and are used as boundary conditions for the model. These measured impedances are also presented.

17. Key Words (Suggested by Author(s))	18. Distribution Statement
Acoustic measurement; Aeroacoustics; Combustion noise; Combustion noise modeling; Impedance measurement	Unclassified - unlimited STAR Category 71

19. Security Classif. (of this report)	20. Security Classif. (of this page)	21. No. of pages	22. Price*
Unclassifed	Unclassified	73	A04

*For sale by the National Technical Information Service, Springfield, Virginia 22161

NASA-Langley, 1983